

Earthquake Scaling Equations Under Small Strain, Steady Moment Release-Rate Conditions in Southern Andes from 2015 to 2017

Patricio A. Toledo¹, Cristián E. Siegel¹, Benoit Derode², Raul Madariaga³, and Jaime M. Campos⁴

¹Universidad de Chile

²Institut de Recherche en Astrophysique et Planétologie

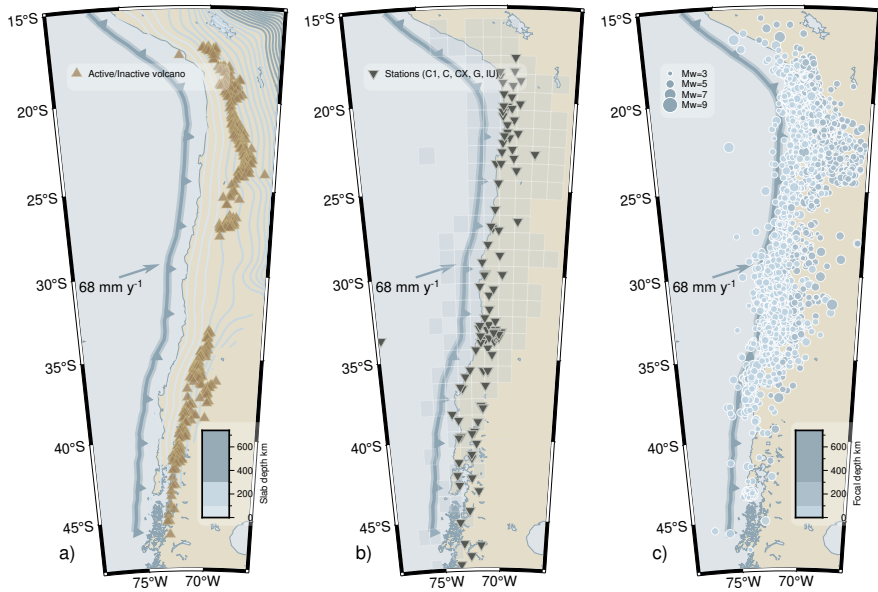
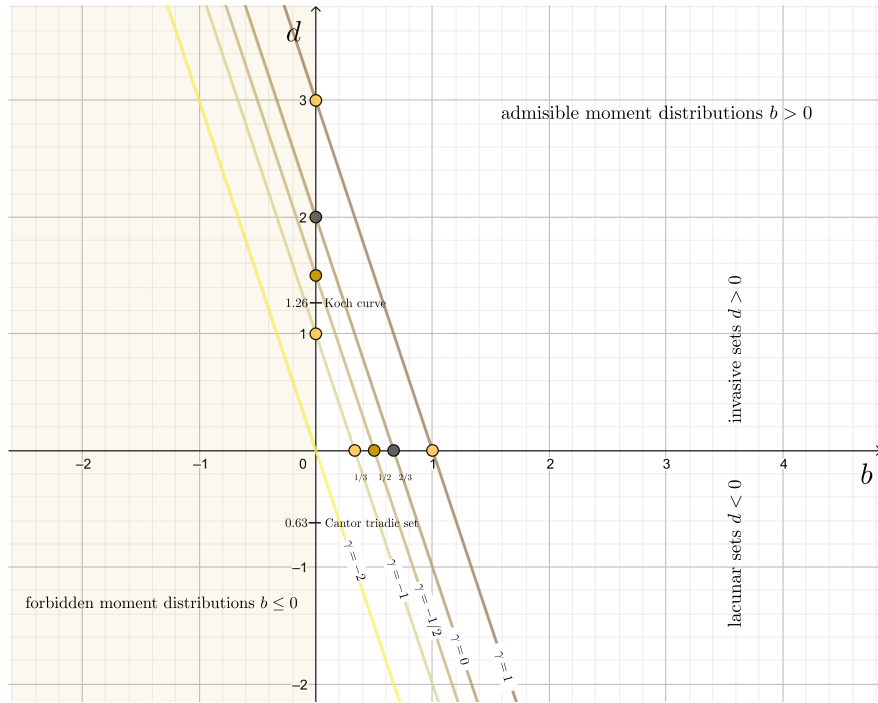
³Ecole Normale Supérieure

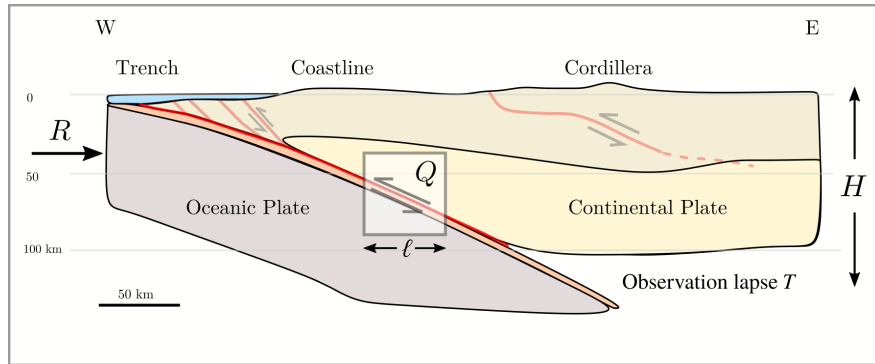
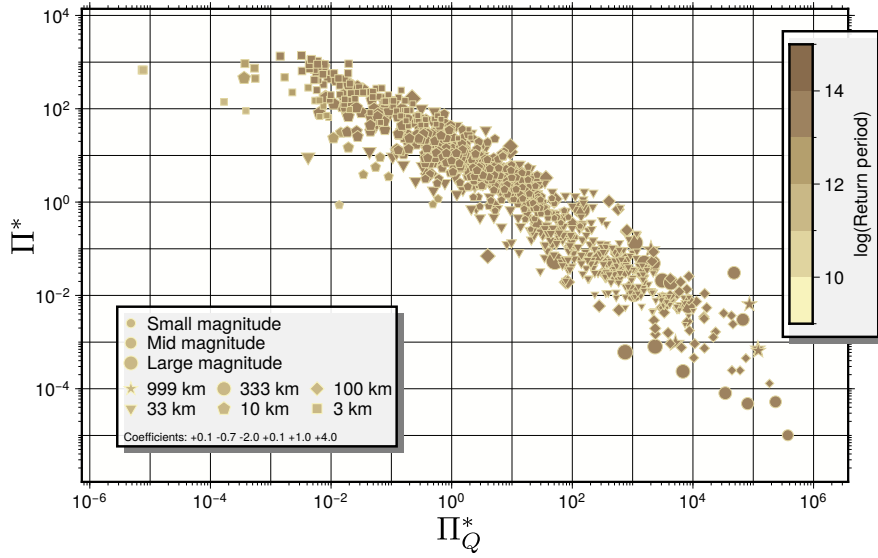
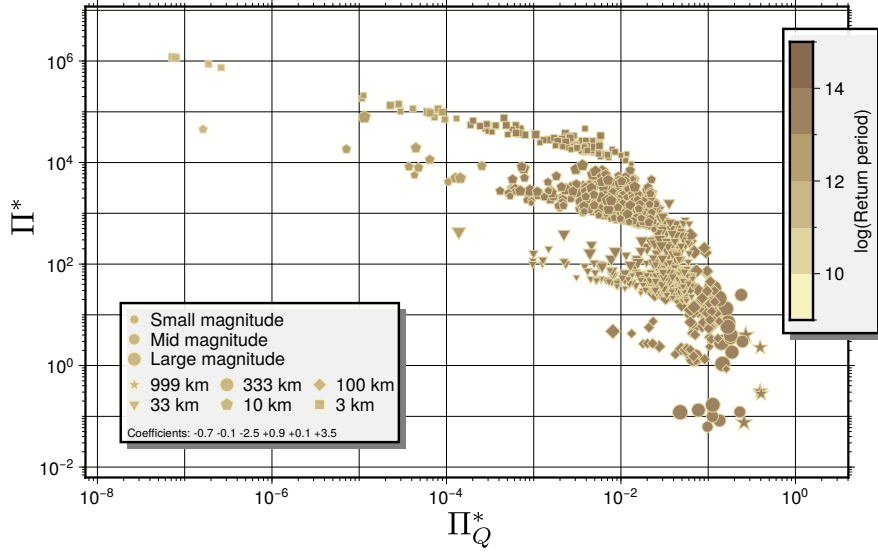
⁴University of Chile

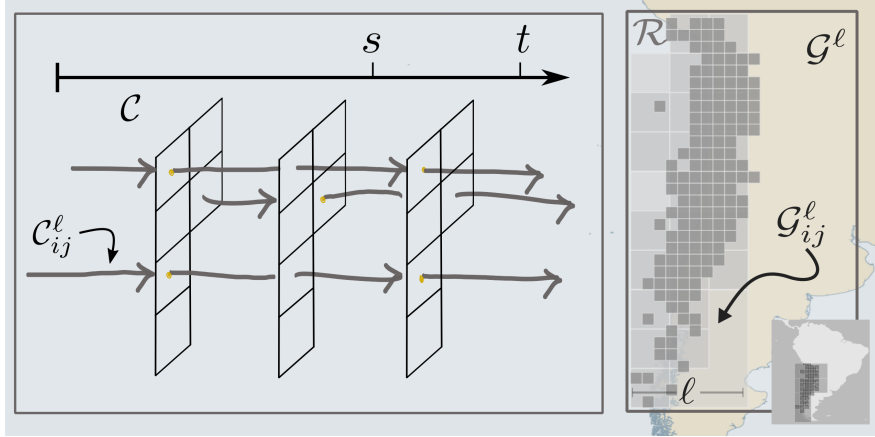
February 20, 2023

Abstract

In the South Andes western edge, a very active seismic contact, with earthquakes up to magnitude 9.5 and ca. 4000 km extension threatens cities and very large populations. The existence of modern seismological networks along the contact allowed the observation of unprecedented earthquake cycle characteristics, which can improve our ability to estimate earthquake hazard, a main objective of seismology. Using dimensional and similarity analysis techniques, we show precise mechanical conditions under which the earthquake generation process unfolds, and derive a set of scaling equations linking renormalized variables. Later on, we test our theoretical results using a curated earthquake point-catalog by using gridding, box-counting, statistical bootstrap and fixed-point iteration collapse techniques. We found non-trivial scaling laws valid across multiple orders of magnitude capable of describing a complex interplay between renormalized earthquake occurrence and renormalized moment release rate. We discuss finite-strain and seismic-moment release-rate conditions; declustering, foreshock, mainshock, aftershock notions; cutoff magnitudes, earthquake hazard implications and a possible large-scale tectonic energy transfer mechanism.







1 **Earthquake Scaling Equations Under Small Strain,**
2 **Steady Moment Release-Rate Conditions in Southern**
3 **Andes from 2015 to 2017**

4 **Patricio A. Toledo¹, Cristián Siegel^{1,3}, Benoit Derode⁴, Raúl Madariaga^{1,2},**
5 **Jaime Campos^{1,3}**

6 ¹Programa de Riesgo Sísmico PRS, Universidad de Chile, Blanco Encalada 2002, Santiago, Chile.

7 ²Département de Géologie, Ecole Normale Supérieure, PSL University, 75005 Paris, France.

8 ³Departamento de Geofísica, Facultad de Ciencias Físicas y Matemáticas, Universidad de Chile, Beauchef
9 850, Santiago, Chile.

10 ⁴Institut de Recherche en Astrophysique et Planétologie, 14 Avenue Edouard Berlin, 31400 Toulouse,
11 France.

12 **Key Points:**

- 13 • We derived a set of scaling equations linking renormalization variables for earth-
14 quake generation processes
- 15 • We found scaling laws valid across multiple orders of magnitude
- 16 • Analyzing statistical (seismic laws) imbrications highlights the importance of the
17 method for large-scale earthquake hazard

Corresponding author: Cristián Siegel, cristian.siegel@uchile.cl

Abstract

In the South Andes western edge, a very active seismic contact, with earthquakes up to magnitude 9.5 and ca. 4000 km extension threatens cities and very large populations. The existence of modern seismological networks along the contact allowed the observation of unprecedented earthquake cycle characteristics, which can improve our ability to estimate earthquake hazard, a main objective of seismology. Using dimensional and similarity analysis techniques, we show precise mechanical conditions under which the earthquake generation process unfolds, and derive a set of scaling equations linking renormalized variables. Later on, we test our theoretical results using a curated earthquake point-catalog by using gridding, box-counting, statistical bootstrap and fixed-point iteration collapse techniques. We found non-trivial scaling laws valid across multiple orders of magnitude capable of describing a complex interplay between renormalized earthquake occurrence and renormalized moment release rate. We discuss finite-strain and seismic-moment release-rate conditions; declustering, foreshock, mainshock, aftershock notions; cutoff magnitudes, earthquake hazard implications and a possible large-scale tectonic energy transfer mechanism.

Plain Language Summary

Earthquakes are the most destructive natural hazard affecting the western edge of South America. If precise earthquake generation conditions are known, then effective public policies might be put in place. In this work, we review practical issues and theoretical aspects of the earthquake generation process and we propose simple relationships between the observable variables at world-wide Seismological Centers. This relationships might be used by decision takers and other scientists as well to advance societal well-being.

1 Introduction

At the western edge of South America two plates subduct, the Nazca Plate to the north and the Antarctic Plate to the south (Ranero et al., 2006). This configuration defines the Southern Andes as one of the seismic zones with the greatest extension and seismic activity, far exceeding 4000 km long, where earthquakes up to magnitude 9.5 (Ruiz & Madariaga, 2018) have been recorded. In Chile, this condition directly affects large communities. For instance Camus et al. (2016) estimated in 11 million the affected population in 2010 only. Therefore, knowing the behavior of seismicity presents a fundamental scientific challenge, and at the same time a practical public policy issue. The precise determination of statistical laws and conditions under which the earthquake generation process unfolds requires theory and experimental observations with positive implications in earthquake hazard analysis. Taking advantage of the unique opportunity that this geographic area represents, during the last decades large instrumental network-installation and maintenance efforts have been made, that have made possible to build earthquake point-catalogs allowing exploration of previously unobserved properties. Therefore, it is expected that these new observations will lead to new extended laws that will improve our understanding of the processes occurring in the crust, and ultimately improve our ability to estimate earthquake hazard.

Our paper is organized as follows: In Section 2 we describe the problem of seismicity generation framed in a seismic-moment loading-unloading cycle. Then we describe precise conditions, based on observations, to simplify the problem and make the main similarity assumptions. Section 3 describes the scaling equations describing the cycle. This set of equations represent the correlations developed as the seismicity phenomenon unfolds. Section 4 presents a review of the tectonic context in which the scaling equations are intended to be applied, and describes the existing instrumentation and data set. Subsequently, the main methodological and statistical elements used to process the

68 earthquake point-catalog information are indicated. In Section 5 the results are presented
 69 and the main scaling characteristics describing the existing correlations are shown. Fi-
 70 nally, in Section 6, the implications are reviewed and discussed.

71 **2 Problem setting**

72 As the Earth crust is the place where the earthquake generation process takes place,
 73 let us consider a region \mathcal{R} (Figure 1) where the main elements in consideration are set.
 74 Let us parameterize the crust by considering the class of systems of units ELT, where
 75 units of energy, length and time are used to describe the quantities of interest. We sup-
 76 pose that the crust is characterized by a seismogenic thickness H . A certain power R —
 77 the main source of available energy— is injected into the crust from the heat flux through
 78 Earth mantle and it is applied at ocean expansion rifts over a very long time T , as a tec-
 79 tonic loading process. A fraction Q of the injected power R is freed when crust-faults
 80 slip a certain amount u releasing a stress-drop $\Delta\sigma$, producing earthquakes whose sizes
 81 are measured through a scalar seismic-moment Mo . Therefore Q represents a seismic-
 82 moment release rate. In general Q is different from R , inducing a proper interevent time
 83 distribution $\tau = Mo/R$, associated with earthquake recurrence phenomena, which can
 84 be consecutive events located in the same place (first-return events) or scattered events
 separated at a distance ℓ within the region bounds (all-return events).

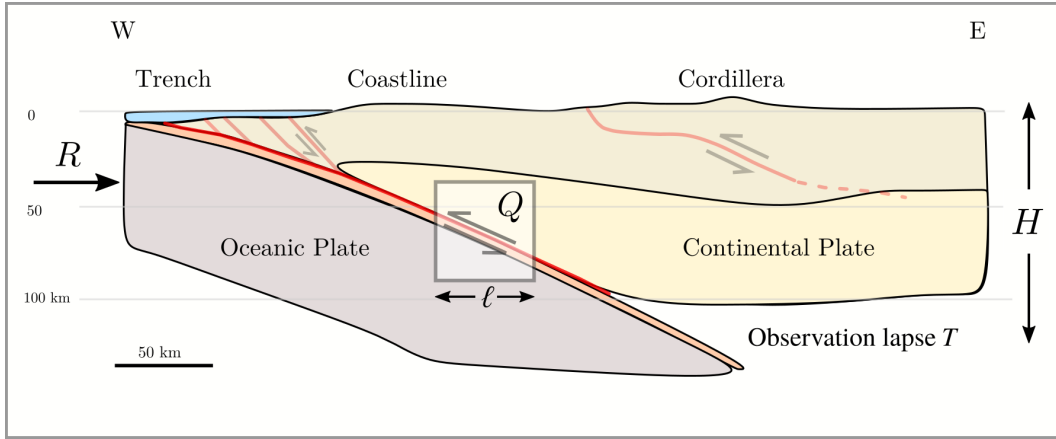


Figure 1. Cross section sketch of a subduction border. An energy injection is placed west with a power R , feeding a complex tectonic process with characteristic geomorphologies (trench, coastline and cordillera) induced by a Continental Plate overriding an Oceanic Plate. Within a volume with proper-length ℓ , a release process Q takes place across a larger volume with proper-length H . The observation period T determines the longer time periods available for study.

85

86 Therefore, as a hazard approximation, we wish to estimate the number of events
 87 per unit time and unit area n taking place in the given geographic region of interest \mathcal{R} ,
 88 during the observation period T given by a general relation φ linking n and the afore-
 89 said parameters:

$$n = \varphi(\ell, \tau, \Delta\sigma, T, Mo, H, u, Q). \quad (1)$$

90 Table 1 shows powers of the dimension function for each parameter, for instance, the di-
 91 mensions of the number of events distribution are $[n] = L^{-2} T^{-1}$, the dimensions of the
 92 stress-drop are $[\Delta\sigma] = EL^{-3}$, the dimension of the interevent distance is $[\ell] = L$, and
 93 the dimension of the interevent time is $[\tau] = T$.

Table 1. Powers of the dimension function in the ELT class for each parameter used in text.

	n	ℓ	τ	$\Delta\sigma$	T	Mo	H	u	Q
E	0	0	0	1	0	1	0	0	1
L	-2	1	0	-3	0	0	1	1	0
T	-1	0	1	0	1	0	0	0	-1

Thus, the number of events distribution n is a function of 8 parameters. As ELT has 3 independent units, there are 3 quantities with dimensions that might be considered independent, let us choose $\Delta\sigma$, ℓ and τ . Therefore, there are $m = 5$ parameters with dependent dimensions. According to dimensional analysis (Sedov, 1993) a function Φ exists such that:

$$\frac{n}{\ell^{-2}\tau^{-1}} = \Phi\left(\frac{T}{\tau}, \frac{Mo}{\Delta\sigma\ell^3}, \frac{H}{\ell}, \frac{u}{\ell}, \frac{Q}{\Delta\sigma\ell^3\tau^{-1}}\right), \quad (2)$$

which is a general result obtained from units alone. In mathematical terms, Φ is symmetric with respect to a group of transformations defining change from one system of units to another within a given class of systems of units. In physical terms, meaningful laws cannot depend on the choice of units, therefore it must be possible to express them using relationships between quantities that do not depend on this arbitrary choice, i.e. dimensionless combinations of variables.

Let us introduce the dimensionless quantities:

$$\begin{aligned} \Pi &= \frac{n}{\ell^{-2}\tau^{-1}}, & \Pi_T &= \frac{T}{\tau}, & \Pi_{Mo} &= \frac{Mo}{\Delta\sigma\ell^3}, \\ \Pi_H &= \frac{H}{\ell}, & \Pi_u &= \frac{u}{\ell}, & \Pi_Q &= \frac{Q}{\Delta\sigma\ell^3\tau^{-1}}, \end{aligned}$$

The relation (2) might then be expressed as follows:

$$\Pi = \Phi(\Pi_T, \Pi_{Mo}, \Pi_H, \Pi_u, \Pi_Q), \quad (3)$$

If we would like to obtain the earthquake occurrence probability distribution, that is to say to sample the distribution Π , we should explore a space of 5 dimensions, one for each dimensionless quantity. If we consider 10 independent observations to estimate the expected value of these dimensionless quantities, we get that an earthquake point-catalog should have at least 10^5 observations, reasonable smaller than 10^8 elements of the original formulation in equation (1).

2.1 Complete similarity conditions

On a physical level a parameter is considered essential, i.e. governing the phenomenon, if the value of the corresponding dimensionless parameter is not too large or not too small (about 0.1 and 10). Thus, let $l \leq m$ define a subset of the parameters. If the dimensionless parameters Π_{l+1}, \dots, Π_m are small or large, it is assumed by convention that the influence of these dimensionless parameters, and consequently of the corresponding dimensional parameters, can be neglected (for a discussion and theorems sustaining this procedure see Barenblatt, 2003). If these conditions are actually satisfied for sufficiently small or sufficiently large Π_{l+1}, \dots, Π_m the function $\Phi(\Pi_1, \dots, \Pi_l, \Pi_{l+1}, \dots, \Pi_m)$ can be replaced by a function Φ^* with fewer arguments:

$$\Pi = \Phi^*(\Pi_1, \dots, \Pi_l). \quad (4)$$

In such cases, we speak of *complete similarity* or *similarity of the first kind* of a phenomenon in the parameters Π_{l+1}, \dots, Π_m (Barenblatt, 1987).

125 The observational period T and the interevent times τ define Π_T which is the in-
 126 verse of Deborah number De , used in very-short or very-long term rheology experiments (Huilgol
 127 & Phan-Thien, 1997; Mendecki, 1996). Deborah number is the ratio between the char-
 128 acteristic relaxation (response) time of a body subjected to a load, and the process loading-
 129 time duration itself, thus for $De \ll 1$ the body behaves like a liquid and for $De \gg 1$ like
 130 a solid. The parameter Π_T poses a very common problem in seismology and geodesy,
 131 while the tectonic energy-dissipation process spans millions of years, modern earthquake
 132 point-catalogs are decades long (Mueller, 2019). Although historical data might increase
 133 the period to hundreds of years (Lomnitz, 1970, 2004; Udías et al., 2012) and paleoseis-
 134 mology to thousands (Cisternas et al., 2012; Vargas et al., 2014) in most scenarios Π_T
 135 is very large. In practice, for an open period we cannot know, a priori, which events have
 136 interevent times smaller than the observation period, at least for causal phenomena. This
 137 parameter cannot be neglected.

138 The dimensionless parameter Π_{Mo} is discussed (at length) by Golitsyn (2007, 2001).
 139 The factor $Mo/\Delta\sigma$ represents, according to Tsuboi (1940, 1956), a volume where seis-
 140 micity takes place. Thus, every earthquake is endowed with a proper-length scale $\sqrt[3]{Mo/\Delta\sigma}$ (Aki,
 141 1972; Kostrov, 1974). It has been known for a while the remarkable low fluctuations of
 142 $\Delta\sigma$, and various scaling laws can be derived from this observation (Kanamori & Ander-
 143 son, 1975; Aki, 1967). A common value for stress-drop is $\Delta\sigma \simeq 4$ MPa (Allmann & Shearer,
 144 2009), thus if stress-drop is nearly constant, then the seismic-moment should scale with
 145 the cube of this length scale (Madariaga, 1979) and Π_{Mo} is expected to fluctuate heav-
 146 ily in earthquake point-catalog surveys, and then cannot be neglected.

147 The parameter Π_H plays a role similar to Knudsen Kn number in statistical physics (Rapp,
 148 2016). It is the ratio of seismogenic thickness H controlling the spatial region of inter-
 149 est and the interevent distance ℓ . For most earthquake pairs ℓ will be small compared
 150 to H , so Π_H should be very large, but long-range space correlations (Kagan & Knopoff,
 151 1980) implies that a considerable number of earthquake pairs will have interevent dis-
 152 tances comparable with the seismogenic thickness, therefore Π_H remains essential (Aki,
 153 1996) and cannot be neglected.

154 The dimensionless parameter Π_Q represents the seismic-moment release-rate pro-
 155 cess. On the global scale Q was estimated to be around 1.2×10^{13} W (Golitsyn, 2001).
 156 The parameter Q governs the earthquake load-release cycle. The product τQ might be
 157 interpreted as the seismic-moment released at the time scale τ whereas the product τR
 158 represents the injected energy at the same time period. Thus the ratio R/Q might be
 159 interpreted as the balance between crustal work inducing loading and crustal work in-
 160 ducing release, the energy budget responsible for the seismic cycle should display a deficit
 161 if $R/Q < 1$ and equilibrium if $R = Q$ and a surplus otherwise. Precise earthquake point-
 162 catalogs should display fluctuations in Π_Q and cannot be neglected.

163 The fault slip u is a parameter that scales with the seismic-moment with a power-
 164 law (Aki, 1972) thus Π_u is not expected to be constant, but as long as the interevent dis-
 165 tance ℓ remains long enough compared with fault slip, this parameter, that represents
 166 a finite strain, will be small. It is therefore natural to introduce a *first similarity hypoth-*
 167 *esis* regarding small finite strains and propose a further simplification of equation (3):

$$\Pi = \Phi^* (\Pi_T, \Pi_{Mo}, \Pi_H, \Pi_Q), \quad (5)$$

168 i.e. based on observational facts, we claim there is complete similarity in the param-
 169 eter Π_u . We expect therefore the function Φ to converge —fast enough— to a non-zero
 170 limit Φ^* when the aforementioned dimensionless quantity goes to zero.

171 2.2 Incomplete similarity conditions

172 The situation just described is far from being the general case. According to Barenblatt
 173 (2003) when the dimensionless parameters Π_{l+1}, \dots, Π_m go to zero or infinity the func-

174 tion Φ does not necessarily tends to a limit. Therefore, the physical parameters remain
 175 essential, no matter how small or large the values of the corresponding dimensionless pa-
 176 rameters Π_{l+1}, \dots, Π_m are. It just happens that there exists another class of phenom-
 177 ena, wider that the class of *complete similarity* phenomena, where the function Φ have
 178 at large or small values of Π_{l+1}, \dots, Π_m the property of generalized homogeneity in its
 179 own dimensionless arguments:

$$\Phi = \Pi_{l+1}^{\alpha_{l+1}} \dots \Pi_m^{\alpha_m} \Phi^* \left(\frac{\Pi_1}{\Pi_{l+1}^{\beta_1} \dots \Pi_m^{\delta_1}}, \dots, \frac{\Pi_l}{\Pi_{l+1}^{\beta_l} \dots \Pi_m^{\delta_l}} \right), \quad (6)$$

180 where $\alpha_{l+1}, \dots, \alpha_m, \beta_1, \dots, \delta_l$ are unknown exponents. We remind that equation (3) comes
 181 from (group) covariance of meaningful physical laws under units change, on the other
 182 hand the generalized homogeneity of equation (6) is a particular property. The expo-
 183 nents cannot be obtained, even in principle, by dimensional considerations, i.e. they are
 184 not universal and they depend on specific conditions of the problem under study. The
 185 parameters Π_{l+1}, \dots, Π_m —which are violating complete similarity— do not disappear
 186 from the analysis, they continue to remain essential, no matter how large or small its sim-
 187 ilarity parameters are. We say the solutions *scale* with the dimensionless quantities Π_{l+1}, \dots, Π_m .
 188 As proposed by Zel'dovich (1956), in such cases we speak of *incomplete similarity* or *sim-*
 189 *ilarity of the second kind* in the relevant parameter. Often, the exponents are obtained
 190 by fitting experimental results, observations, or by numerical modeling. They tend to
 191 be real non-rational values, physicists call these exponents *anomalous dimensions* (Wilson,
 192 1975, 1979) and the scaling procedure bears the name *renormalization* (Kadanoff, 1966)
 193 which is a by-product of covariance of Φ^* under rescaling of its own dimensionless ar-
 194 guments (Goldenfeld, 1992).

195 Beginning with the work of Bak et al. (2002); Christensen et al. (2002) and the pre-
 196 cursory research of Kossobokov and Mazhkenov (1994) a systematic generalization of earth-
 197 quake scaling relations took place. It is now recognized that a wider set of laws rule the
 198 seismic-moment release-rate process in the crust (Corral, 2003). Equation (5) expresses
 199 earthquake occurrence statistics under very restricted (complete) similarity conditions.
 200 Extensive observational data describing long-period interevent time correlations (Omori,
 201 1894; Utsu et al., 1995; Ogata, 1988) suggests that there is incomplete similarity in the
 202 parameter Π_T under conditions of large (and small) values of the dimensionless param-
 203 eter, that is:

$$\Pi = \Pi_T^\alpha \Phi^* \left(\frac{\Pi_{M_0}}{\Pi_T^{\alpha_{M_0}}}, \frac{\Pi_H}{\Pi_T^{\alpha_H}}, \frac{\Pi_Q}{\Pi_T^{\alpha_Q}} \right), \quad (7)$$

204 where $\alpha, \alpha_{M_0}, \alpha_H$ and α_Q are real-valued exponents. Analogous conditions over seismic-
 205 moment dimensionless parameter Π_{M_0} are well known (Gutenberg & Richter, 1956):

$$\Pi = \Pi_T^\alpha \Pi_{M_0}^\beta \Phi^* \left(\frac{\Pi_H}{\Pi_T^{\alpha_H} \Pi_{M_0}^{\beta_H}}, \frac{\Pi_Q}{\Pi_T^{\alpha_Q} \Pi_{M_0}^{\beta_Q}} \right), \quad (8)$$

206 where β, β_H , and β_Q are real-valued exponents also. Similar evidence regarding long-range
 207 interevent distance correlations (Kagan & Knopoff, 1980; Scholz & Aviles, 1986; Okubo
 208 & Aki, 1987), as well as (renormalization) group symmetries (Corral, 2005) suggests that
 209 under conditions of large (or small) values of the similarity parameter Π_H , incomplete
 210 similarity exists, that is:

$$\Pi = \Pi_T^\alpha \Pi_{M_0}^\beta \Pi_H^\gamma \Phi^* \left(\frac{\Pi_Q}{\Pi_T^{\alpha_Q} \Pi_{M_0}^{\beta_Q} \Pi_H^{\gamma_Q}} \right), \quad (9)$$

211 with γ and γ_Q real-valued exponents. Rearranging terms, a symmetrical form might be
 212 obtained that can be interpreted in terms of renormalized parameters only:

$$\Pi^* = \Phi^*(\Pi_Q^*), \quad (10)$$

213 where Π^* is the renormalized event number and Π_Q^* is the renormalized seismic-moment
 214 release-rate number. Thus, the equation (10) represents a *second similarity hypothesis*,
 215 regarding long-range correlation conditions. We must remark that exponents $\alpha, \beta, \gamma, \alpha_Q, \beta_Q,$
 216 and γ_Q define the number of events distribution given the particular seismic conditions
 217 (interevent times, interevent distances, seismic-moment, seismic-moment release-rate),
 218 tectonic conditions (stress-drop and seismogenic width) and other region-dependant pa-
 219 rameters (observation period). Note that constancy of Q lead us to a hypothesis regard-
 220 ing steady seismic-moment release-rate conditions.

221 3 Scaling equations

222 Going back to the original variables in equation (10) we might write:

$$n\tau^p Mo^b \ell^d = f(\tau^{p_Q} Mo^{b_Q} \ell^{d_Q}), \quad (11)$$

223 where f is a scaling function depending on tectonic conditions at play. Moreover, a set
 224 of relationships between the unknown exponents associated with renormalization group
 225 symmetries and exponents associated with the physical parameters might be obtained:

$$\begin{cases} p &= \alpha + 1, & b &= -\beta, & d &= 3\beta + \gamma + 2, \\ p_Q &= \alpha_Q + 1, & b_Q &= -\beta_Q, & d_Q &= 3\beta_Q + \gamma_Q - 3. \end{cases} \quad (12)$$

226 This conditions are termed scaling relations, and represent fundamental objects in crit-
 227 ical phenomena theory (Widom, 2009). The exponent p is related to Omori law, d is re-
 228 lated to epicenters fractal dimension and b is related to seismic moment scaling. When
 229 Φ^* is linear, exponents p_Q, d_Q and b_Q are reduced to Omori, Gutenberg-Richter and frac-
 230 tal laws. Power law behavior is a very special case, and tapered exponential has long been
 231 advocated (Kagan, 1994). By inspection of (12) it can be said that interevent-times ex-
 232 ponents are independent in contrast to interevent-distances and seismic-moment release-
 233 rate exponents, which are always related. Note that while p should be positive (nega-
 234 tive) so that a decay (increase) in events number follows increasing (decreasing) interevent
 235 times, b and d are more complex. Aki (1981) stated two scenarios for faults: linear ob-
 236 jects filling a surface ($1 < d < 2$), or planar objects filling a volume ($2 < d < 3$). Work-
 237 ing on disordered materials Carpinteri and Chiaia (1997) suggested two scenarios in fa-
 238 tigue cycles, a loading process defined over lacunar (Cantor-like) sets where progressive
 239 void-appearance speeds-up failure by stress concentration, and a release process defined
 240 over invasive (Koch-like) sets where progressive detail-appearance speeds-up dissipation
 241 by surface-energy build-up. As seen in Figure 2 there is ample space for those scenar-
 242 ios depending on γ values. For instance, if $\gamma = -1$ then invasive sets with dimension
 243 $d < 1$ support moment distributions as long as $b \leq 1/3$. On the contrary lacunar sets oc-
 244 cur for $b > 1/3$, and values of $\gamma = -2$ are always associated with lacunar sets, as long
 245 as $b > 0$.

246 4 Southern Andes tectonic framework, data and statistical techniques

247 As shown in Figure 3a Nazca plate advances at 68 mm y^{-1} (Norabuena et al., 1998)
 248 in N76E direction (Angermann et al., 1999) with respect to South America, forming a
 249 convergent contact. The trace of convergence (trench) is roughly aligned NS at the greater
 250 bathymetric depths. Under the continent, the northern subducting plate segment shows
 251 a simple but abrupt morphology up until 33°S (Contreras-Reyes et al., 2012), correlat-
 252 ing with a tectonic erosive regime along the overriding plate base. The southern segment
 253 shows a flattened subduction plate and a tectonic accretionary border that reaches up
 254 until 45°S where an erosive regime develops again. Further south, the Pacific Plate
 255 subduces South America at 18 mm y^{-1} under accretionary conditions not fully understood
 256 yet (Ranero et al., 2006). The volcanic arc (mostly) follows the aforementioned tectonic
 257 regimes with active volcanoes distributed along the Andes with a sharp gap between 30

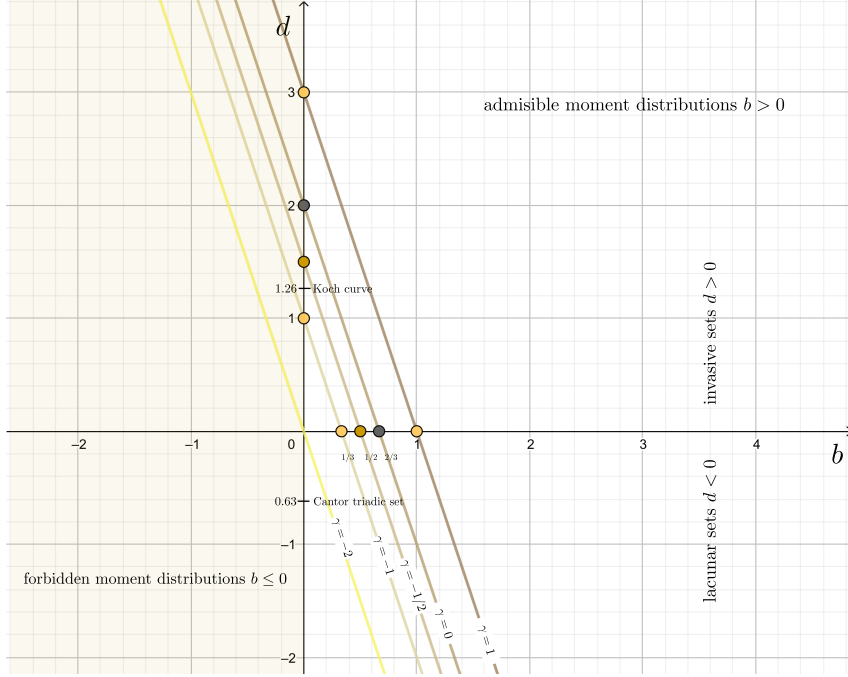


Figure 2. Scaling laws representing the relationship between b and d for various values of γ . Admissible values for b are positive, while d values can be positive (invasive sets) or negative (lacunar sets). Laws with $\gamma \leq -2$ always represent lacunar sets for b positive, laws with $-2 \leq \gamma \leq -1$ represent lacunar sets for $b \leq 1/3$ and invasive sets for $b > 1/3$. Fractal dimensions for Koch curve and Cantor triadic set are shown as reference.

258 and 35°S (Ranero et al., 2006). From 2001 onwards various earthquakes with magnitudes
 259 greater than 7.0 have been recorded. Northern notable earthquakes are the 2005 Mw 7.8
 260 Tarapacá earthquake, the 2007 Mw 7.8 Tocopilla earthquake, the 2007 Mw 7.7 Iquique
 261 earthquake and the great 2014 Mw 8.2 Iquique earthquake. Central South Andes has not
 262 presented earthquakes greater than 6 after 2001, but extensive swarms have been recorded.
 263 Southern notable earthquake are 2001 Mw 7.0 Papudo earthquake, the great 2010 Mw 8.8
 264 Maule earthquake, the 2011 Mw 7.1 Arauco earthquake, the great 2015 Mw 8.3 Illapel
 265 earthquake and the 2016 Mw 7.6 Chiloé earthquake. A thorough description of these events
 266 can be found in Ruiz and Madariaga (2018). Figure 3b shows the station network man-
 267 aged by the Plate Boundary Observatory (IPOC), Geoscope, the Global Seismograph
 268 Network (GSN) and the Chilean National Seismological Center (CSN). A variety of in-
 269 struments compose the network. Derode et al. (2019) reports the use of modern broad-
 270 band and accelerometers distributed across the western South Andes border. Thus, there
 271 is spatial covering homogeneity but heterogeneous instrumental capacity. In Figure 3c
 272 the earthquake point-catalog used in this study is shown, where 6274 earthquakes were
 273 analyzed with FMNEAR method (Delouis, 2014) from January 1st, 2015 until Decem-
 274 ber 31, 2017. Earthquake hypocenters with shallow depth near the trench represent ca. 60%
 275 of the catalog whereas 30% are intermediate-depth events (> 70 km), occurring mostly
 276 north of 25°S latitude, with prominence between 19 and 23°S . Maximum estimated earth-
 277 quake depth is 390 km while magnitudes range between Mw 1.7 and 7.8, (see Derode et
 278 al., 2019, for further details).

279 The main data analysis tool is the gridding and box-counting technique (Feder, 2013)
 280 as shown in Figure 4, right panel. The region \mathcal{R} is covered by a bidimensional grid \mathcal{G}^ℓ
 281 composed of proper-length ℓ cells \mathcal{G}_{ij}^ℓ , where $i, j = 1, 2, \dots$ are positional indices. The

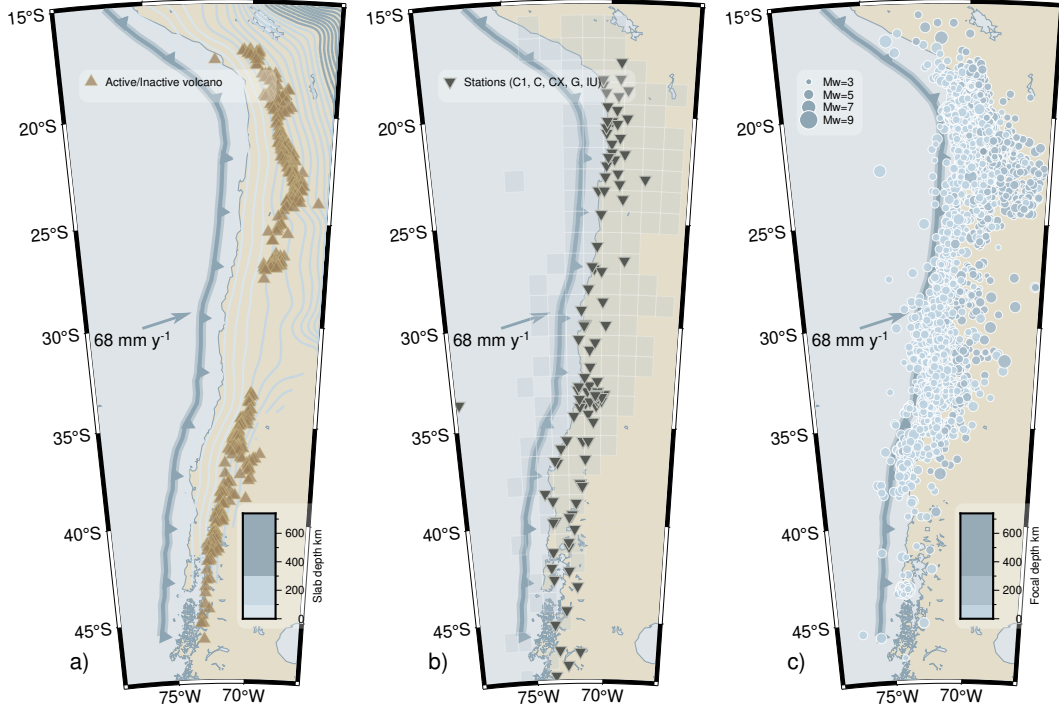


Figure 3. Tectonic, network and earthquake point-catalog context. Left a) plane view of western South America. The subduction trace (trench) is roughly axial to coast line. The Nazca plate advances at 68 mm y^{-1} long-term velocity. A volcanic arc appears parallel to coastline with a remarkable gap correlated with a flatter subduction interface (colored isobath lines). Center b) The seismic network being operated, also a grid with cells covering the region of interest. Right c) Seismicity during 2015-2017 period as published by (Derode et al., 2019).

282 intersection of an earthquake point-catalog \mathcal{C} with \mathcal{G}^ℓ generates subcatalogs \mathcal{C}_{ij}^ℓ as illus-
 283 trated in Figure 4, left panel. These subcatalogs represent a deformation field which is
 284 a mathematical object that might be described by a punctuated random-field process,
 285 with earthquakes acting as points scattered at a distances always shorter than ℓ within
 286 \mathcal{G}_{ij}^ℓ . To ensure small finite strain conditions a cutoff must be imposed on every event in
 287 every subcatalog. We built the cells matching the typical earthquake source radius $r^3 = \frac{7}{16} \frac{M_0}{\Delta\sigma}$
 288 from Madariaga (2020) and we selected only those events with estimated radius smaller
 289 than cell proper-length ℓ , under these conditions Π_u is small and the first similarity hy-
 290 pothesis is always fulfilled.

Table 2. Grid characteristics used in the study, see Figure 4 and Figure 3b.

	\mathcal{G}^ℓ					
Cell Length ℓ , km	3	10	33	100	333	1000
Magnitude cutoff	5	6	7	8	9	10
Min return period, s	3.59×10^3	2.87×10^3	1.02×10^5	4.60×10^5	8.11×10^5	1.46×10^6
Max return period, s	9.24×10^7	9.37×10^7	9.40×10^7	9.46×10^7	9.46×10^7	9.46×10^7
Number of cells	4848	2498	688	154	29	4

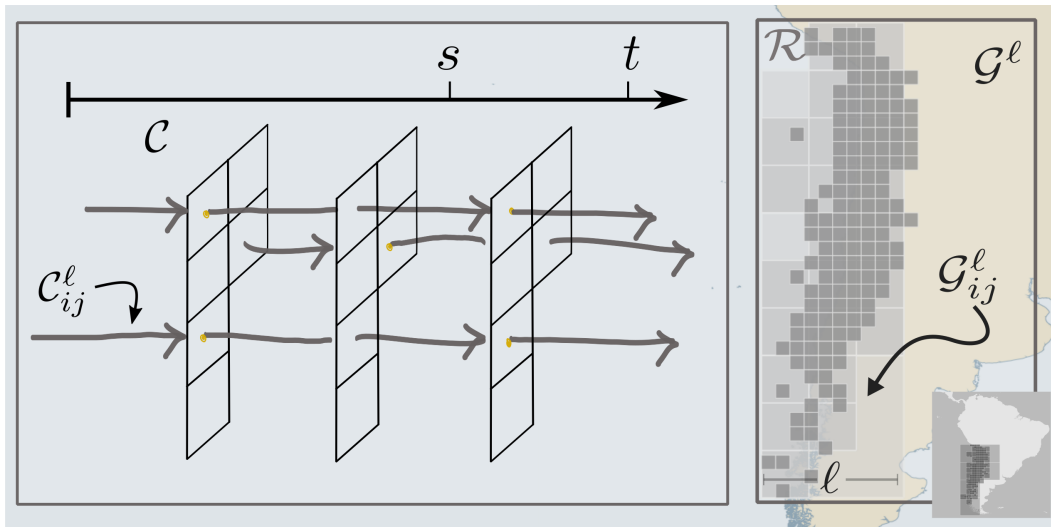


Figure 4. Earthquake point-catalog sketch and gridding-technique. An earthquake point-catalog might be intersected with a grid \mathcal{G}^{ℓ} covering a region \mathcal{R} . An evolution process marked at specific points in time s and t where earthquakes occur is induced, thereby creating a subcatalog \mathcal{C}_{ij}^{ℓ} for every cell \mathcal{G}_{ij}^{ℓ} within the grid. As different proper scales ℓ are explored, the process precise description changes.

291 We used 6 grids, having cell (edge) proper-lengths between 3–1000 km, see Table 2
 292 for specific characteristics. The grid with cells ca. 100 km proper-length is shown in Figure 3 b.
 293 For every subcatalog \mathcal{C}_{ij}^{ℓ} the governing parameters seismic-moment released M_0 ,
 294 interevent distances ℓ and interevent times τ are analyzed. Statistical estimators collected
 295 at every scale are cell maximal seismic-moment, cell maximal interevent distances and
 296 cell average interevent times (see tabulated statistics in Toledo et al., 2023). We must
 297 remark that average interevent times coincides with homogeneous Poisson process un-
 298 biased maximum-likelihood rate estimator, thus subcatalogs with 4 events or more are
 299 retained, although only 3 points minimum a required by theory.

300 This choice of maximal bounds avoids the use of binned density histograms, there-
 301 fore we obtain cumulative experimental histograms which are more stable than density
 302 statistics known as source of problems in power law data (Virkar & Clauset, 2014) and
 303 also smears a known bias when fitting logarithmic data with least squares (Goldstein et
 304 al., 2004). Note that Gutenberg-Richter balance exponent b_{GR} is defined with respect
 305 to survival (complementary cumulative) magnitudes (Serra & Corral, 2017), and as we
 306 collect cumulative seismic-moments, we have $b = \frac{2}{3}b_{\text{GR}}$. Also note that cumulative ex-
 307 perimental histograms avoids $1 + \beta$ exponents that are source of confusions (Kagan, 1994).

308 The scaling function Φ^* in equation (11) is unknown, and supposing a power law
 309 translate the problem to a careful exponent estimation using constrained optimization
 310 fit (Branch et al., 1999). From a seed around expected exponents, 2500 iterations are
 311 produced each time sampling 25% of the data, so that mean values with 2σ reverse boot-
 312 strap percentile intervals (Diaconis & Efron, 1983; Efron & Tibshirani, 1994) are reported.
 313 We understand this fitting process as a collapse procedure—that is fixed point itera-
 314 tions using the renormalization group—in search for the special situation where all data
 315 fall-in a single curve that represents a stable point in the parametric space see Houdayer
 316 and Hartmann (2004).

Table 3. Scaling exponents as shown in Figure 6 and 5. Referential seismogenic thickness $H = 1.00 \times 10^5$ m, observation period $T = 9.46 \times 10^7$ s (3 years) stress-drop $\Delta\sigma = 4.00 \times 10^6$ Pa, and seismic-moment release-rate $Q = 1.00 \times 10^{12}$ W.

	α	β	γ	α_Q	β_Q	γ_Q
theory [†]	+0.1	$-\frac{2}{3}$	-2	+0.1	$+\frac{2}{3}$	+3
uncollapsed [•]	-0.7	-0.1	-2.5	+0.9	+0.1	+3.5
collapsed [‡]	$+0.09050^{+0.00009}_{-0.00014}$	-0.66	$-1.99063^{+0.00014}_{-0.00016}$	$0.10952^{+0.00009}_{-0.00013}$	0.99	$3.99063^{+0.00014}_{-0.00012}$

[†] See β values in Kagan (1994), α fits $p \simeq 1$ and γ a non-fractal surface. [‡] this study, [•] non physical.

317 Finally, a consideration is to be made regarding fractal dimension. In this case the
 318 calculated exponents corresponds to bidimensional box-counting dimension d_{BC} , which
 319 is an upper limit for Hausdorff dimension d_H (Ott, 2002), therefore $d_H \leq d_{BC}$.

320 5 Results

321 First order statistics are shown in Table 2. There are 6 grids with cell proper-lengths
 322 3, 10, 33, 100, 333 and 1000 km, the number of cells decrease from 4848 at proper-length
 323 3 km to 4 at proper-length 1000 km, representing a lacunar fractal with dimension 1.24.
 324 The grid with proper-length 3 km, i.e. containing events with interevent distances ℓ no
 325 greater than 3 km and cutoff Mw 5, show average interevent return times τ from $3.59 \times$
 326 10^3 s to 9.24×10^7 s, a range from minutes to years. The grid with cell proper-length
 327 10 km shows the same long-period range. The grid with cell proper-length 33 km show
 328 an interevent return times range from 1.02×10^5 s to 9.40×10^7 s, a range from days to
 329 years. Grids with proper-lengths 100 and 333 km show the same long-period range. Fi-
 330 nally the grid with proper-length 1000 km, cover the study area with 4 cells, have min-
 331 imum average return period of 1.46×10^6 s and maximum average return period $9.46 \times$
 332 10^7 s, a range from weeks to years.

333 In Figures 5 and 6 the collapse process is shown. The situation in Figure 5 is not
 334 physically admissible. Very low γ and β (see exponents in Table 3) values are translated
 335 into a global trend with renormalized event number Π^* decreasing with renormalized seismic-
 336 moment release-rate Π_Q^* . Interevent return times τ (color encoded) display an inverse trend,
 337 same with interevent distances ℓ (symbol encoded). But note the splitting pattern where
 338 different symbols do not mix at mid to lower Π_Q^* values, meaning that no unique scal-
 339 ing function Φ^* can describe the situation. Also note that for each symbol (each length
 340 scale ℓ) a corner can be seen, meaning that this particular set of exponents is not able
 341 to describe the renormalized event distribution within its boundaries. In Figure 6 a dif-
 342 ferent situation is shown. A single inverse relationship between Π_Q^* and Π^* is displayed.
 343 There is considerable scatter, but a general trend where data from all scales involved col-
 344 lapse. As expected from a stable point, seismic-moment β exponent do not display ap-
 345 preciable variance to be reported, as seen in Table 3. Likewise α and γ also present small
 346 variability and both of them show a slight positive-skewness. The low p -value is consis-
 347 tent with our selection of (Poisson) interevent times estimator, moreover there are re-
 348 markable long-period correlations as seen in the strong overlapping.

349 Considering the large catalog extent, scaling exponents should be taken as aver-
 350 aged values, as fluctuations are present when considering each grid alone. These expo-
 351 nents are not crust parameters, they depend on the problem at hand, including its bound-
 352 ary conditions, so that specific places with different values are perfectly possible. A sin-
 353 gle scaling function Φ^* , fitting data across Southern Andes, with power-law shape might
 354 be proposed, but we do not rule out a tapered or other scaling laws. Indeed, a gentler

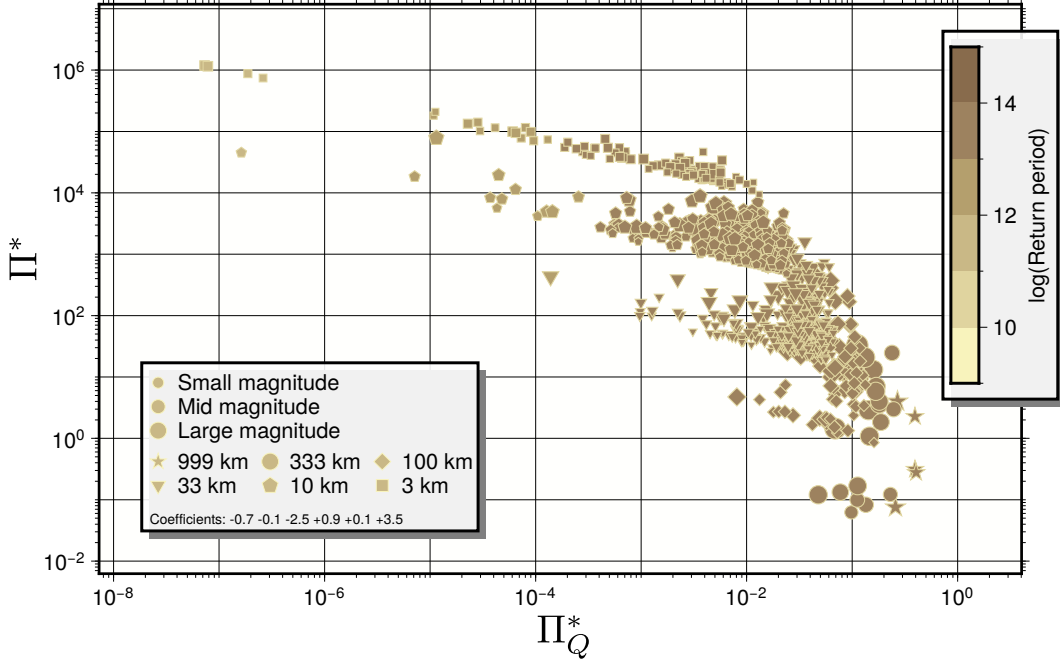


Figure 5. Uncollapsed scaling situation. Renormalized event number Π^* decrease with renormalized seismic-moment release-rate Π_Q^* . Note the clear splitting with interevent length ℓ , meaning that no scaling function Φ^* can describe the situation, and also note that for each curve a corner might be identified in Π_Q^* axis, meaning that this set of exponents is not able to describe the renormalized event distribution. Exponents as shown in Table 3. Referential seismogenic thickness $H = 1.00 \times 10^5$ m, observation period $T = 9.46 \times 10^7$ s (3 years) stress-drop $\Delta\sigma = 4.00 \times 10^6$ Pa, and seismic-moment release-rate $Q = 1.00 \times 10^{12}$ W.

355 slope might be seen at renormalized seismic-moment release-rates around $\Pi_Q^* \simeq 1$, mean-
 356 ing that complex structures are still hidden.

357 6 Discussion and conclusions

358 Similarity hypothesis. Considering the first similarity hypothesis about small-strain
 359 condition over Π_u , i.e. the condition on fault-displacements smaller than the proper scale
 360 ℓ , it might be said that there exists a prominent asymptotic (complete) similar solution
 361 as seen in the collapse reached by the curves indexed by ℓ . Further analysis will require
 362 a catalog with variables regarding processes with scales smaller than ℓ , that is the in-
 363 formation from the physics at the seismic source. Considering the second similarity hy-
 364 pothesis, confirmed in view of the large dynamical range achieved by the renormalized
 365 parameters with a single set of exponents fitting a reasonably well behaved function Φ^* .
 366 Other earthquake point-catalogs, with longer observational periods, larger magnitude
 367 ranges and longer interevent-distances, should be studied to further confirm this hypoth-
 368 esis. Regarding the steady seismic-moment release-rate condition over Π_Q we can repeat
 369 the last argument. However, as suggested by Benzi et al. (2022), a steady seismic-moment
 370 release-rate is a variable affecting interevent time distributions, to further explore it we
 371 should relax the conditions over Π_Q and put back the injection rate R into the formu-
 372 lation, thus a catalog describing slow phenomena is then needed.

373 Griding and box-counting technique. Two main consequences might be extracted:
 374 1) The natural declustering process taking place when dimensionless interevent-distances

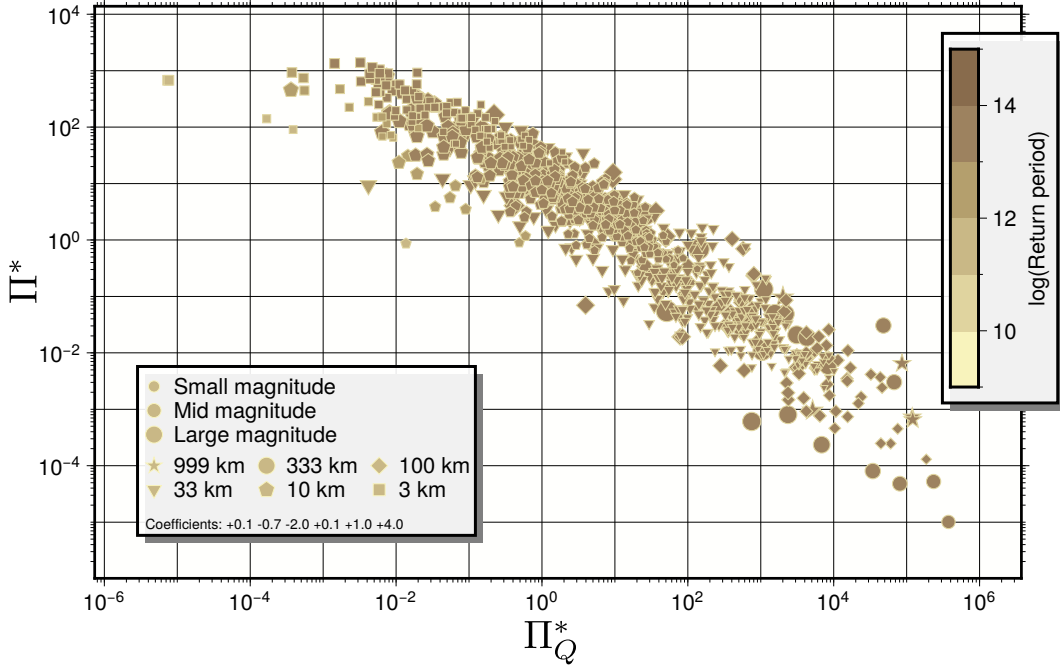


Figure 6. Collapsed scaling situation. Note the transition from gentler to steeper slopes near $\Pi_Q^* \simeq 1$, and also the nice collapsing across 10 orders of magnitude with strong overlapping, which is critical in earthquake hazard estimation. Exponents as shown in Table 3. Referential seismicogenic thickness $H = 1.00 \times 10^5$ m, observation period $T = 9.46 \times 10^7$ s (3 years) stress-drop $\Delta\sigma = 4.00 \times 10^6$ Pa, and seismic-moment release-rate $Q = 1.00 \times 10^{12}$ W.

375 are considered. As there is no complete similarity in Π_H , the long-range correlations be-
 376 tween event distances never disappear, so that given a cell proper-length ℓ , it induces
 377 a working grid \mathcal{G}^ℓ and, in a natural way, the subcatalog creation process assure that all
 378 events placed at the maximal distance ℓ are taken into account. Because of the long-range
 379 correlations, this interevent distances have a considerable effect on the renormalized earth-
 380 quake distributions. This fact is connected with distance declustering as proposed by Baiesi
 381 and Paczuski (2004), which take us directly to the second consequence: 2) The subcat-
 382 alog creation process induce a time reordering. The idea of foreshock, mainshock and
 383 aftershock is explicitly defined. These temporal concepts have meaning only when a proper
 384 scale ℓ is previously given. One event might be aftershock or foreshock only at a fixed
 385 proper scale ℓ at a given cell belonging to a given grid, thus the long-range interevent-
 386 distances influences the long-range interevent-times. This is a general feature observed
 387 in various materials subjected to different mechanisms when thresholds are applied, see
 388 Janićević et al. (2016) for recent theoretical and experimental research.

389 **Magnitude cutoff.** The completeness of an earthquake point-catalog, that is the lower
 390 magnitude cutoff assuring a Gutenberg-Richter law, is related to the dimensionless mo-
 391 ment Π_{M_0} . There is no unique cutoff assessment-procedure (Mignan & Woessner, 2012)
 392 because an independent relationship is needed. The parameter estimation used here is
 393 an alternative and it must be pursued in future works. No general micro-physical earth-
 394 quake model can satisfactorily account for our fixed-point renormalized iteration, there-
 395 fore no clear resolution is given here.

396 **Homogeneity and isotropy.** Other earthquake point-catalog characteristics that should
 397 be explored, in the proposed context, is dependence with respect to space-translation and

398 grid-azimuth of the renormalized event number Π^* , this is a delicate issue because our
 399 implicit notion of statistical homogeneity is only local, at the cell-grid level. Same thing
 400 can be said with regards to isotropy. In close relation to space-translation is depth de-
 401 pendence. As our grid analysis is bidimensional, all depth variations are lost, so various
 402 tectonic features are not incorporated. Future analysis should deal with these shortcom-
 403 ings.

404 Seismic cycle. The notion of seismic cycle has a proper-length scale attached to it,
 405 naturally the largest scale is intensely studied because it determines the maximum cred-
 406 ible earthquake, a relevant notion in hazard studies. For example, on the western edge
 407 of the Andes, between 18 and 24°S latitude Métois et al. (2013) have established a se-
 408 ries of segments, whose proper-lengths are believed to have some predictive power when
 409 analyzing the geodetic coupling. Similarly between 26 and 30°S latitude, there is a well
 410 known segment, quiescent since the 1922 *Mw* 8.6 earthquake (Ruiz & Madariaga, 2018).
 411 These segments, approximately 500 km, are associated with return periods ca. 100 years
 412 therefore it is natural to inquire about the relevance of the earthquake point-catalog stud-
 413 ied, which covers a region from 18 to 45° S latitude and only 3 years long. The key idea
 414 is renormalization, i.e. the process by which the governing parameters are rescaled by
 415 means of exponents obtained from the observations. This process respects the relation-
 416 ship that is believed to exist between the segments (a proper-length scale), the seismic
 417 gap (a proper-time scale) and the magnitude of the earthquake that is expected in the
 418 gap (a proper-size scale) by extending this relationship to the whole data in the cata-
 419 log, thus the gridding technique comprehensively covers the observable proper lengths,
 420 influencing the interevent times and seismic moment distributions, resulting in stable cat-
 421 alog properties such as those observed in Figure 6. Take for example events in cells ca. 333 km
 422 represented by circles and those cells ca. 999 km shown as stars. Although most circles
 423 and stars are at the right edge of Figure 6, at high Π_Q^* values, it is also true that there
 424 is mixing, this phenomenon is due to the collapse/renormalization process which induces
 425 a rearrangement when compared to Figure 5, where stars and circles are not mixed. It
 426 follows that inferences on the boundaries of Π_Q^* have been influenced by data in the other
 427 scales, i.e. there is an uncertainty reduction, especially where errors by extrapolation oc-
 428 cur.

429 Tectonics. The average exponent values correspond to $p = 1.09$, $b_{GR} = 0.99$, and
 430 $d_{BC} = -1.97$, that is the renormalized event number represent a seismic moment release
 431 distribution with decaying (near) hyperbolic interevent times and lacunar-set support,
 432 denser than a Koch curve. Therefore, as indicated by Carpinteri and Chiaia (1997), the
 433 2015-2017 Southern Andes situation is one of loading. By the time of the 1995 *Mw* 8.5
 434 Antofagasta earthquake, Sobiesiak (2000) reported $b_{GR} = 0.73$ over the fault plane with
 435 peaks at 0.54 and 1.08. Pastén and Comte (2014) gave a multifractal series converging
 436 to $d_\infty = 1.45$, so our values are higher on average, however those numbers have a local
 437 character. A recent global survey by Nishikawa and Ide (2014) reports b_{GR} values at six
 438 sections located between 19.8°S and 34.2°S latitude. Peaks range from $b_{GR} = 0.79$ to 0.94
 439 with a decreasing north-south trend. These values are in good accord with our findings.
 440 Finally Poulos et al. (2019) gives values between $b_{BR} = 0.87$ and $b_{GR} = 1.04$ for their
 441 zones 1 and 5, which are also consistent with our findings. More important is the phys-
 442 ical significance of the joint scaling spanning ten orders of magnitude hinting at a *grand*
 443 process taking place from cortical mega-scale down to single-fault meso-scale.

444 Cascade of energy. Clearly, no energy transfer process is at play when passing from
 445 one proper scale to another. This scenario is analog to the cascade mechanism in tur-
 446 bulence (Batchelor, 1947) where vortices are created (or destroyed) without energy loss
 447 as long as the fluid is confined in an *inertial range* where vortices are small compared
 448 to the fluid proper-length scale. The inertial range in turbulence is a region delimited
 449 by two length boundaries: First, a lower limit such that viscous dissipation processes takes
 450 place on smaller scales and second, an upper limit such that forcing processes take place

451 on larger scales. The energy transfer process between this scales is characterized by a
 452 viscous-free energy rate dissipation spectra decaying as $\ell^{-5/3}$ (Kolmogórov, 1941). If the
 453 analogy stands, there must be a physical scale λ where earthquake source micro-processes
 454 taking place at scales smaller than λ might be considered stationary, so that no seismic-
 455 moment transfer mechanism takes place when going up to scales larger than λ . In other
 456 words, as long as the first similarity hypothesis over Π_u is fulfilled, no seismic-moment
 457 is released when passing from one scale to another. Likewise, there must be a mechan-
 458 ical scale where seismic-moment transfer processes between scales ceases to be dissipa-
 459 tion free. A larger scale $\Lambda = \sqrt[3]{Q/(\Delta\sigma T^{-1})} \simeq 300$ km is a candidate, but further stud-
 460 ies are needed. Note the relevance of the observation period, while Q is supposed con-
 461 stant (steady seismic-moment release rate hypothesis) and $\Delta\sigma$ is by large a stable prop-
 462 erty, T is a catalog property and until we reach very long observation periods, spanning
 463 various earthquake cycles the energy cascade upper boundary cannot be known with rea-
 464 sonable certainty.

465 Earthquake hazard. The renormalized event number Π^* distribution is a zeroth-
 466 order hazard estimator, in terms of probabilities, the most important issue is the explicit
 467 dependence of scales, not only length scales but also interevent times and magnitude scales,
 468 and more importantly the boundaries where incomplete similarity holds. Earthquake haz-
 469 ard is an explicit function of the power exponents as well, and most importantly of the
 470 given observation period T and tectonic setting—defined by the seismogenic thickness
 471 H , the seismic-moment release-rate Q and the mean stress-drop $\Delta\sigma$ —thus no material
 472 property is involved, all parameters are functions of the particular region under study
 473 i.e. the available earthquake point-catalogs and the specific tectonic conditions. This gen-
 474 eral comment is consistent with common empirical practice in hazard science. Maybe
 475 the functional shape of Φ^* can be shared among different areas, but recent studies have
 476 shown that more complex structures are present when other variables are analyzed, like
 477 earthquake taxonomy where different scalings are observed when epicenter clusters are
 478 organized in clusters (C. Siegel, 2022; C. E. Siegel et al., 2022).

479 Acknowledgments

480 PT, CS, RM and JC acknowledge financial support from the Seismic Risk Program (PRS).
 481 We thanks IPOC collaboration affiliated institutions (German Research Center For Geo-
 482 sciences (GFZ), Germany; GEOSCOPE Program of Institut de Physique du Globe de
 483 Paris and C.N.R.S., France; Centro Sismológico Nacional (CSN) of Faculty of Physical
 484 and Mathematical Sciences of University of Chile; and Universidad Católica del Norte,
 485 Chile) GFZ German Research Centre For Geosciences and Institut Des Sciences De L’Univers-
 486 Centre National De La Recherche CNRS-INSU (2006); Barrientos (2018) for the seis-
 487 mic network maintenance that made this work possible.

488 Figures were made with GMT (Wessel et al., 2019) and Inkscape. Gridding tech-
 489 nique was implemented with GRASS GIS (Neteler et al., 2012). Catalog analysis were
 490 made with Numpy (Harris et al., 2020).

491 **Data availability:** Original and processed data available at (Toledo et al., 2023).

492 References

- 493 Aki, K. (1967). Scaling law of seismic spectrum. *Journal of Geophysical Research*,
 494 *72*(4), 1217–1231.
 495 Aki, K. (1972). Earthquake mechanism. *Tectonophysics*, *13*(1-4), 423–446.
 496 Aki, K. (1981). A probabilistic synthesis of precursors phenomena. In *Earthquake*
 497 *prediction* (p. 566-574). American Geophysical Union (AGU). Retrieved from
 498 <https://agupubs.onlinelibrary.wiley.com/doi/abs/10.1029/ME004p0566>
 499 doi: <https://doi.org/10.1029/ME004p0566>

- 500 Aki, K. (1996). Scale dependence in earthquake phenomena and its relevance to
 501 earthquake prediction. *Proceedings of the National Academy of Sciences*,
 502 *93*(9), 3740–3747.
- 503 Allmann, B. P., & Shearer, P. M. (2009). Global variations of stress drop for moder-
 504 ate to large earthquakes. *Journal of Geophysical Research: Solid Earth (1978–*
 505 *2012)*, *114*(B1).
- 506 Angermann, D., Klotz, J., & Reigber, C. (1999). Space-geodetic estimation of the
 507 Nazca-South America Euler vector. *Earth and Planetary Science Letters*,
 508 *171*(3), 329–334.
- 509 Baiesi, M., & Paczuski, M. (2004). Scale-free networks of earthquakes and after-
 510 shocks. *Physical review E*, *69*(6), 066106.
- 511 Bak, P., Christensen, K., Danon, L., & Scanlon, T. (2002). Unified scaling law for
 512 earthquakes. *Physical Review Letters*, *88*(17), 178501.
- 513 Barenblatt, G. I. (1987). *Dimensional analysis*. CRC Press.
- 514 Barenblatt, G. I. (2003). *Scaling*. Cambridge University Press. doi: 10.1017/
 515 CBO9780511814921
- 516 Barrientos, S. (2018). The seismic network of Chile. *Seismological Research Letters*,
 517 *89*(2A), 467–474.
- 518 Batchelor, G. (1947). Kolmogoroff’s theory of locally isotropic turbulence. In
 519 *Mathematical proceedings of the cambridge philosophical society* (Vol. 43, pp.
 520 533–559).
- 521 Benzi, R., Castaldi, I., Toschi, F., & Trampert, J. (2022). Self-similar properties of
 522 avalanche statistics in a simple turbulent model. *Philosophical Transactions*
 523 *of the Royal Society A: Mathematical, Physical and Engineering Sciences*,
 524 *380*(2218), 20210074. Retrieved from [https://royalsocietypublishing](https://royalsocietypublishing.org/doi/abs/10.1098/rsta.2021.0074)
 525 [.org/doi/abs/10.1098/rsta.2021.0074](https://royalsocietypublishing.org/doi/abs/10.1098/rsta.2021.0074) doi: 10.1098/rsta.2021.0074
- 526 Branch, M.-A., Coleman, T., & Li, Y. (1999). A subspace, interior, and conjugate
 527 gradient method for large-scale bound-constrained minimization problems.
 528 *SIAM Journal on Scientific Computing*, *21*(1), 1–23.
- 529 Camus, P., Arenas, F., Lagos, M., & Romero, A. (2016). Visión histórica de la
 530 respuesta a las amenazas naturales en Chile y oportunidades de gestión del
 531 riesgo de desastre. *Revista de Geografía Norte Grande*(64), 9–20.
- 532 Carpinteri, A., & Chiaia, B. (1997). Multifractal scaling laws in the breaking be-
 533 haviour of disordered materials. *Chaos, Solitons & Fractals*, *8*(2), 135–150.
- 534 Christensen, K., Danon, L., Scanlon, T., & Bak, P. (2002). Unified scaling law
 535 for earthquakes. *Proceedings of the National Academy of Sciences*, *99*(suppl 1),
 536 2509–2513.
- 537 Cisternas, M., Torrejón, F., & Gorigoitia, N. (2012). Amending and complicating
 538 Chile’s seismic catalog with the Santiago earthquake of 7 august 1580. *Journal*
 539 *of South American Earth Sciences*, *33*(1), 102–109.
- 540 Contreras-Reyes, E., Jara, J., Grevemeyer, I., Ruiz, S., & Carrizo, D. (2012). Abrupt
 541 change in the dip of the subducting plate beneath north Chile. *Nature Geo-*
 542 *science*, *5*(5), 342.
- 543 Corral, A. (2003). Local distributions and rate fluctuations in a unified scaling law
 544 for earthquakes. *Physical Review E*, *68*(3), 035102.
- 545 Corral, A. (2005). Renormalization-group transformations and correlations of seis-
 546 micity. *Physical review letters*, *95*(2), 028501.
- 547 Delouis, B. (2014). FMNEAR: Determination of focal mechanism and first esti-
 548 mate of rupture directivity using near-source records and a linear distribution
 549 of point sources. *Bulletin of the Seismological Society of America*, *104*(3),
 550 1479–1500.
- 551 Derode, B., Delouis, B., & Campos, J. (2019). Systematic Determination of Focal
 552 Mechanisms over a Wide Magnitude Range: Insights from the Real-Time FM-
 553 NEAR Implementation in Chile from 2015 to 2017. *Seismological Research*
 554 *Letters*, *90*(3), 1285–1295.

- 555 Diaconis, P., & Efron, B. (1983). Computer-intensive methods in statistics. *Scientific*
 556 *American*, *248*(5), 116–131.
- 557 Efron, B., & Tibshirani, R. J. (1994). *An introduction to the bootstrap*. CRC press.
- 558 Feder, J. (2013). *Fractals*. Springer Science & Business Media.
- 559 GFZ German Research Centre For Geosciences, & Institut Des Sciences De
 560 L’Univers-Centre National De La Recherche CNRS-INSU. (2006). *Ipoc seismic*
 561 *network*. Integrated Plate boundary Observatory Chile - IPOC. Retrieved from
 562 <http://geofon.gfz-potsdam.de/doi/network/CX> doi: 10.14470/PK615318
- 563 Goldenfeld, N. D. (1992). *Lectures on phase transitions and the renormalization*
 564 *group*. Addison-Wesley.
- 565 Goldstein, M. L., Morris, S. A., & Yen, G. G. (2004). Problems with fitting to the
 566 power-law distribution. *The European Physical Journal B-Condensed Matter*
 567 *and Complex Systems*, *41*(2), 255–258.
- 568 Golitsyn, G. S. (2001). Place of the Gutenberg-Richter law among other statistical
 569 laws of nature. *Vychislitel’naya Seysmologiya*, *32*, 119–137.
- 570 Golitsyn, G. S. (2007). Energy cycle of geodynamics and the seismic process.
 571 *Izvestiya, Physics of the Solid Earth*, *43*(6), 443–446.
- 572 Gutenberg, B., & Richter, C. F. (1956). Earthquake magnitude, intensity, energy,
 573 and acceleration: (second paper). *Bulletin of the seismological society of Amer-*
 574 *ica*, *46*(2), 105–145.
- 575 Harris, C. R., Millman, K. J., van der Walt, S. J., Gommers, R., Virtanen, P., Cour-
 576 napeau, D., . . . Oliphant, T. E. (2020, September). Array programming with
 577 NumPy. *Nature*, *585*(7825), 357–362. Retrieved from [https://doi.org/](https://doi.org/10.1038/s41586-020-2649-2)
 578 [10.1038/s41586-020-2649-2](https://doi.org/10.1038/s41586-020-2649-2) doi: 10.1038/s41586-020-2649-2
- 579 Houdayer, J., & Hartmann, A. K. (2004). Low-temperature behavior of two-
 580 dimensional Gaussian Ising spin glasses. *Physical Review B*, *70*(1), 014418.
- 581 Huilgol, R. R., & Phan-Thien, N. (1997). *Fluid mechanics of viscoelasticity: gen-*
 582 *eral principles, constitutive modelling, analytical and numerical techniques*. El-
 583 sevier.
- 584 Janićević, S., Laurson, L., Måløy, K. J., Santucci, S., & Alava, M. J. (2016). In-
 585 terevent correlations from avalanches hiding below the detection threshold.
 586 *Physical review letters*, *117*(23), 230601.
- 587 Kadanoff, L. P. (1966). Scaling laws for Ising models near T_c . *Physics Physique*
 588 *Fizika*, *2*(6), 263.
- 589 Kagan, Y. Y. (1994). Observational evidence for earthquakes as a nonlinear dynamic
 590 process. *Physica D: Nonlinear Phenomena*, *77*(1), 160–192.
- 591 Kagan, Y. Y., & Knopoff, L. (1980). Spatial distribution of earthquakes: the two-
 592 point correlation function. *Geophysical Journal International*, *62*(2), 303–320.
- 593 Kanamori, H., & Anderson, D. L. (1975). Theoretical basis of some empirical re-
 594 lations in seismology. *Bulletin of the seismological society of America*, *65*(5),
 595 1073–1095.
- 596 Kolmogórov, A. (1941). Dissipation of energy in locally isotropic turbulence. In *Dok-*
 597 *lady akademii nauk* (Vol. 32, pp. 16–18).
- 598 Kossobokov, V., & Mazhkenov, S. (1994). On similarity in the spatial distribution of
 599 seismicity. *Computational seismology and geodynamics*, *1*, 6–15.
- 600 Kostrov, V. (1974). Seismic moment and energy of earthquakes, and seismic flow of
 601 rock. *Physics of the Solid Earth*, *1*, 13–21.
- 602 Lomnitz, C. (1970). Major earthquakes and tsunamis in Chile during the period
 603 1535 to 1955. *Geologische Rundschau*, *59*(3), 938–960.
- 604 Lomnitz, C. (2004). Major earthquakes of Chile: a historical survey, 1535-1960. *Seis-*
 605 *mological Research Letters*, *75*(3), 368–378.
- 606 Madariaga, R. (1979). On the relation between seismic moment and stress drop in
 607 the presence of stress and strength heterogeneity. *Journal of Geophysical Re-*
 608 *search: Solid Earth*, *84*(B5), 2243–2250.

- 609 Madariaga, R. (2020). Earthquake source theory. *Encyclopedia of Solid Earth Geo-*
610 *physics*, 1–5.
- 611 Mendecki, A. J. (1996). *Seismic monitoring in mines*. Springer Science & Business
612 Media.
- 613 Métois, M., Socquet, A., Vigny, C., Carrizo, D., Peyrat, S., Delorme, A., . . . Or-
614 tega, I. (2013). Revisiting the North Chile seismic gap segmentation using
615 GPS-derived interseismic coupling. *Geophysical Journal International*, *194*(3),
616 1283–1294.
- 617 Mignan, A., & Woessner, J. (2012). Estimating the magnitude of completeness
618 for earthquake catalogs. *Community Online Resource for Statistical Seismicity*
619 *Analysis*, 1–45.
- 620 Mueller, C. S. (2019). Earthquake catalogs for the USGS national seismic hazard
621 maps. *Seismological Research Letters*, *90*(1), 251–261.
- 622 Neteler, M., Bowman, M., Landa, M., & Metz, M. (2012). GRASS GIS: a multi-
623 purpose Open Source GIS. *Environmental Modelling & Software*, *31*, 124–130.
624 doi: 10.1016/j.envsoft.2011.11.014
- 625 Nishikawa, T., & Ide, S. (2014). Earthquake size distribution in subduction zones
626 linked to slab buoyancy. *Nature Geoscience*, *7*(12), 904–908.
- 627 Norabuena, E., Leffler-Griffin, L., Mao, A., Dixon, T., Stein, S., Sacks, I. S., . . .
628 Ellis, M. (1998). Space Geodetic Observations of Nazca-South America
629 Convergence Across the Central Andes. *Science*, *279*(5349), 358–362. Re-
630 trieved from <https://science.sciencemag.org/content/279/5349/358> doi:
631 10.1126/science.279.5349.358
- 632 Ogata, Y. (1988). Statistical models for earthquake occurrences and residual
633 analysis for point processes. *Journal of the American Statistical association*,
634 *83*(401), 9–27.
- 635 Okubo, P. G., & Aki, K. (1987). Fractal geometry in the San Andreas fault system.
636 *Journal of Geophysical Research: Solid Earth (1978–2012)*, *92*(B1), 345–355.
- 637 Omori, F. (1894). On the after-shocks of earthquakes. *J. Coll. Sci., Imp. Univ.,*
638 *Japan*, *7*, 111–200.
- 639 Ott, E. (2002). *Chaos in dynamical systems*. Cambridge university press.
- 640 Pastén, D., & Comte, D. (2014). multifractal analysis of three large earthquakes in
641 Chile: Antofagasta 1995, Valparaíso 1985, and Maule 2010. *Journal of seismol-*
642 *ogy*, *18*(4), 707–713.
- 643 Poulos, A., Monsalve, M., Zamora, N., & de la Llera, J. C. (2019). An updated
644 recurrence model for Chilean subduction seismicity and statistical validation of
645 its Poisson nature. *Bulletin of the Seismological Society of America*, *109*(1),
646 66–74.
- 647 Ranero, C. R., von Huene, R., Weinrebe, W., & Reichert, C. (2006). Tectonic
648 processes along the Chile convergent margin. In *The andes* (pp. 91–121).
649 Springer.
- 650 Rapp, B. E. (2016). *Microfluidics: modeling, mechanics and mathematics*. William
651 Andrew.
- 652 Ruiz, S., & Madariaga, R. (2018). Historical and recent large megathrust earth-
653 quakes in Chile. *Tectonophysics*, *733*, 37–56.
- 654 Scholz, C. H., & Aviles, C. A. (1986). The fractal geometry of faults and fault-
655 ing. In *Earthquake source mechanics* (p. 147-155). American Geophysical
656 Union (AGU). Retrieved from [https://agupubs.onlinelibrary.wiley.com/](https://agupubs.onlinelibrary.wiley.com/doi/abs/10.1029/GM037p0147)
657 [doi/abs/10.1029/GM037p0147](https://agupubs.onlinelibrary.wiley.com/doi/abs/10.1029/GM037p0147) doi: 10.1029/GM037p0147
- 658 Sedov, L. I. (1993). *Similarity and dimensional methods in mechanics*. CRC press.
- 659 Serra, I., & Corral, Á. (2017). Deviation from power law of the global seismic mo-
660 ment distribution. *Scientific reports*, *7*(1), 1–8.
- 661 Siegel, C. (2022). *Propiedades de similitud de catálogos de sismicidad en el con-*
662 *texto tectónico de subducción del Norte Grande de Chile (19° S y 24° S)* (Tesis
663 para optar al grado de magíster en ciencias). Universidad de Chile.

- 664 Siegel, C. E., Toledo, P., Madariaga, R., & Campos, J. (2022). Scaling of waiting
 665 time distribution in northern Chile. *ESS Open Archive*. Retrieved from 10
 666 .1002/essoar.10508115.3
- 667 Sobiesiak, M. M. (2000). Fault plane structure of the Antofagasta, Chile earthquake
 668 of 1995. *Geophysical research letters*, *27*(4), 577–580.
- 669 Toledo, P., Siegel, C., Derode, B., Madariaga, R., & Campos, J. (2023, Jan-
 670 uary). *Earthquake Scaling Equations Under Small Strain, Steady Mo-
 671 ment Release-Rate Conditions in Southern Andes from 2015 to 2017*. Zen-
 672 odo. Retrieved from <https://doi.org/10.5281/zenodo.7644746> doi:
 673 10.5281/zenodo.7644746
- 674 Tsuboi, C. (1940). Isostasy and maximum earthquake energy. *Proceedings of the Im-
 675 perial Academy*, *16*(9), 449–454.
- 676 Tsuboi, C. (1956). Earthquake energy, earthquake volume, aftershock area, and
 677 strength of the Earth’s crust. *Journal of Physics of the Earth*, *4*(2), 63–66.
- 678 Udías, A., Madariaga, R., Buforn, E., Muñoz, D., & Ros, M. (2012). The large
 679 Chilean historical earthquakes of 1647, 1657, 1730, and 1751 from contempo-
 680 rary documents. *Bulletin of the Seismological Society of America*, *102*(4),
 681 1639–1653.
- 682 Utsu, T., Ogata, Y., & Matsu’ura, R. S. (1995). The centenary of the Omori formula
 683 for a decay law of aftershock activity. *Journal of Physics of the Earth*, *43*(1),
 684 1–33.
- 685 Vargas, G., Klinger, Y., Rockwell, T., Forman, S., Rebolledo, S., Baize, S., ...
 686 Armijo, R. (2014). Probing large intraplate earthquakes at the west flank
 687 of the Andes. *Geology*, *42*(12), 1083–1086.
- 688 Virkar, Y., & Clauset, A. (2014). Power-law distributions in binned empiri-
 689 cal data. *The Annals of Applied Statistics*, *8*(1), 90–119. Retrieved from
 690 <http://www.jstor.org/stable/24521727>
- 691 Wessel, P., Luis, J., Uieda, L., Scharroo, R., Wobbe, F., Smith, W., & Tian, D.
 692 (2019). The Generic Mapping Tools version 6. *Geochemistry, Geophysics,
 693 Geosystems*, *20*(11), 5556–5564.
- 694 Widom, B. (2009). Scaling laws. *Scholarpedia*, *4*(10), 9054. doi: 10.4249/
 695 scholarpedia.9054
- 696 Wilson, K. G. (1975). The renormalization group: Critical phenomena and the
 697 Kondo problem. *Reviews of modern physics*, *47*(4), 773.
- 698 Wilson, K. G. (1979). Problems in physics with many scales of length. *Scientific
 699 American*, *241*(2), 158–179.
- 700 Zel’dovich, J. B. (1956). The motion of a gas under the action of a short-term pres-
 701 sure shock. *Soviet Physics Acoustics*, *2*(1), 25–35.

Figure1.

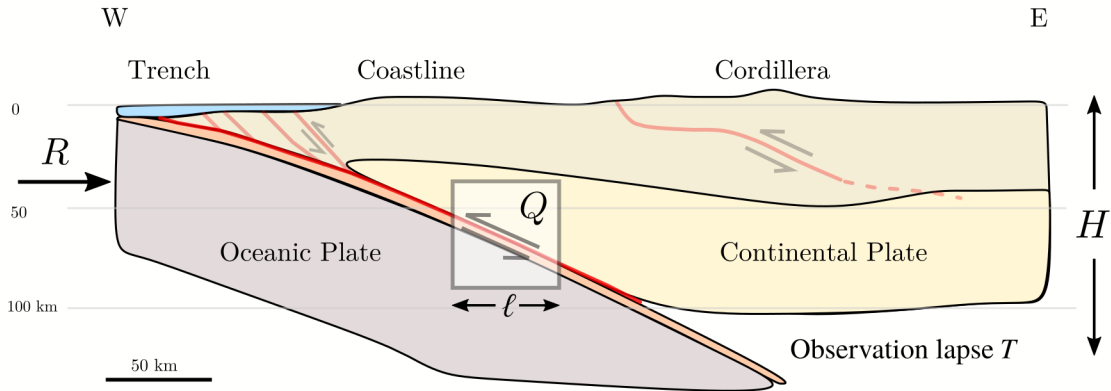


Figure2.

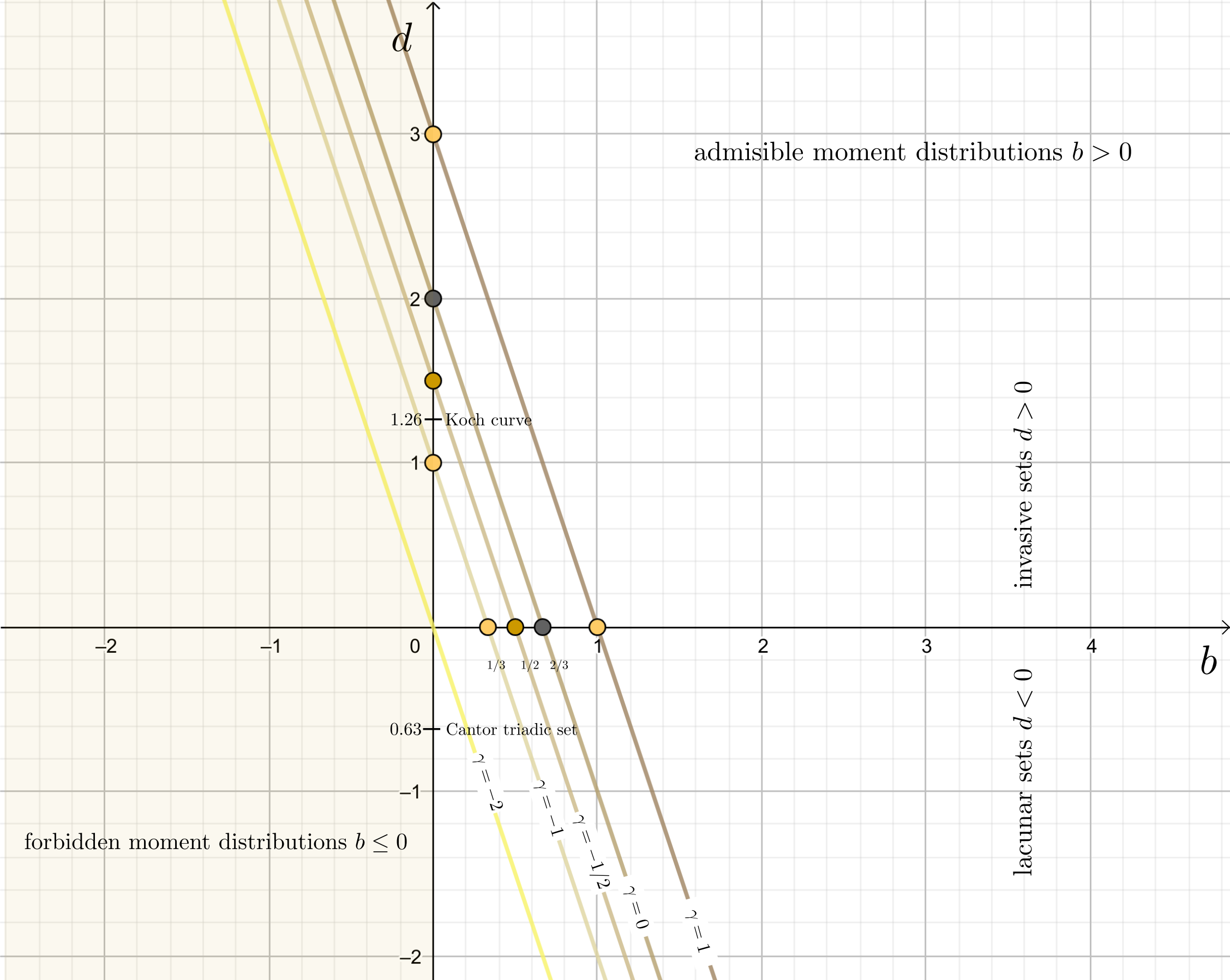


Figure3.

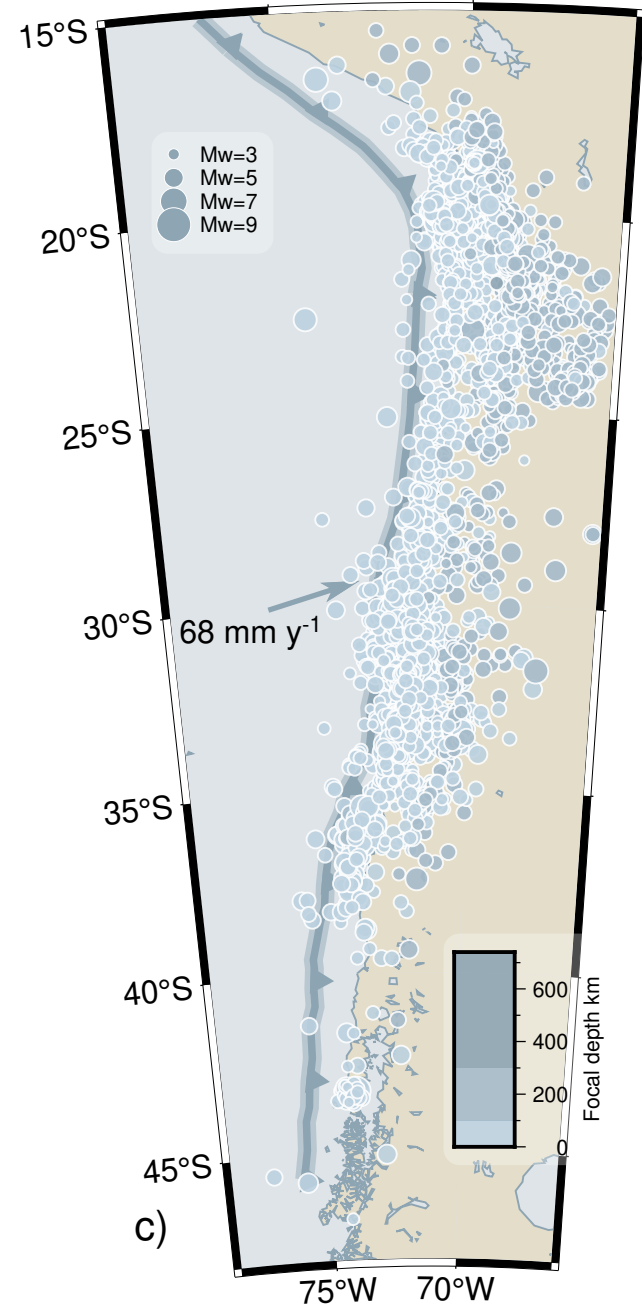
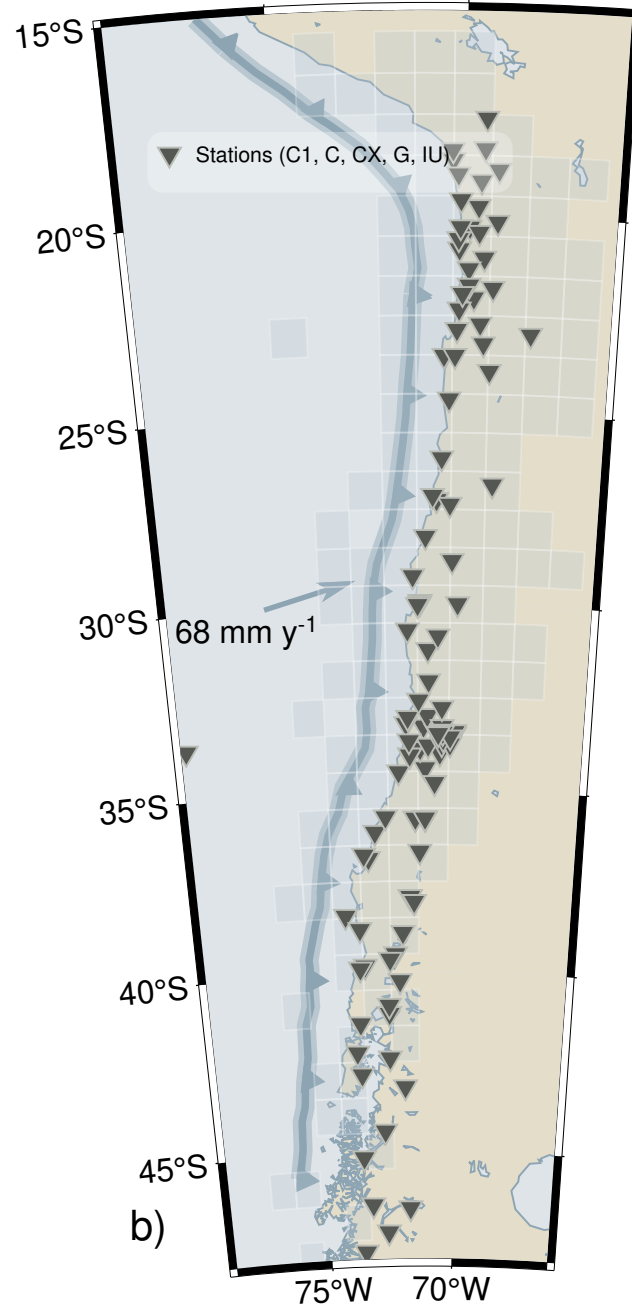
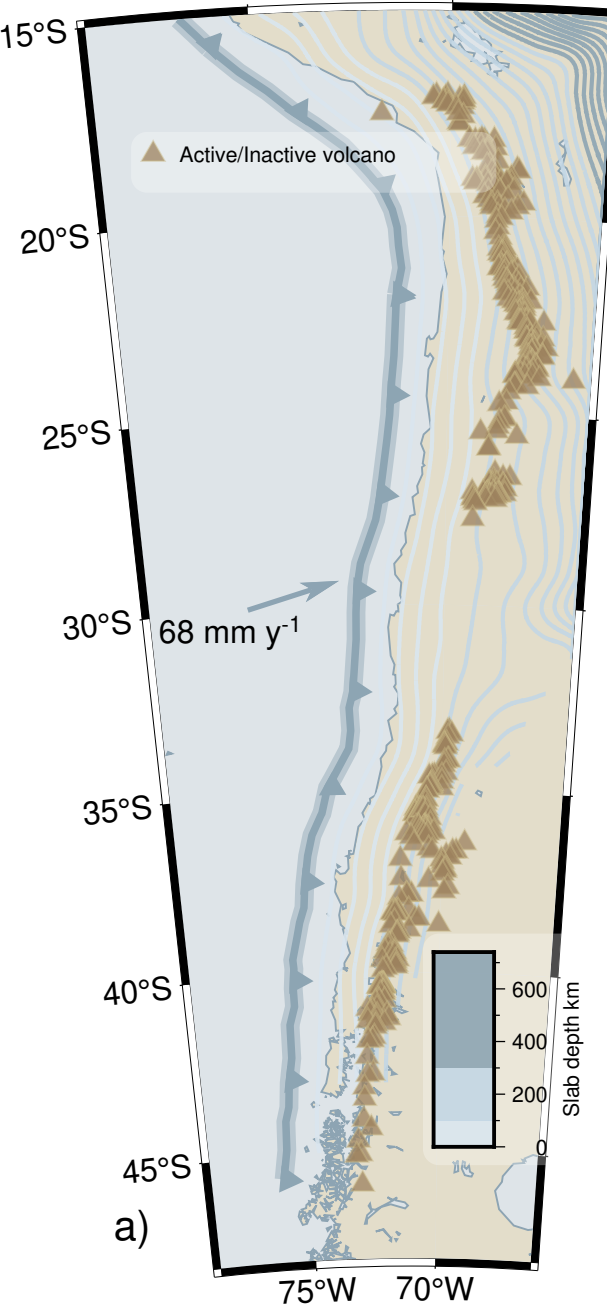


Figure4.

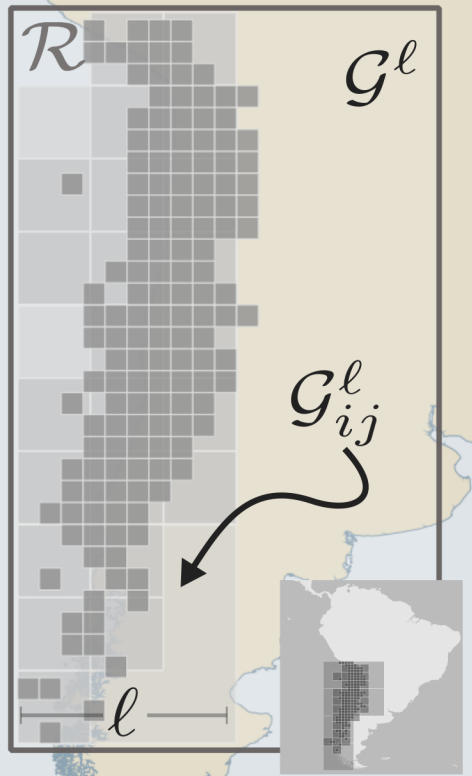
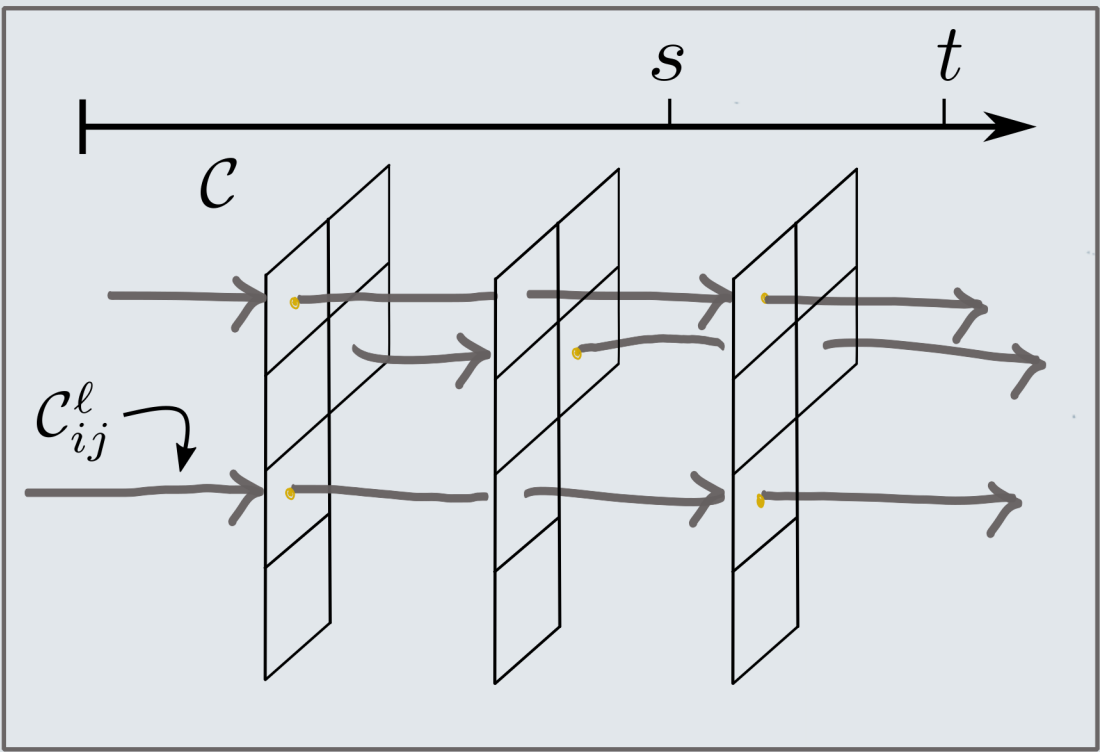


Figure5.

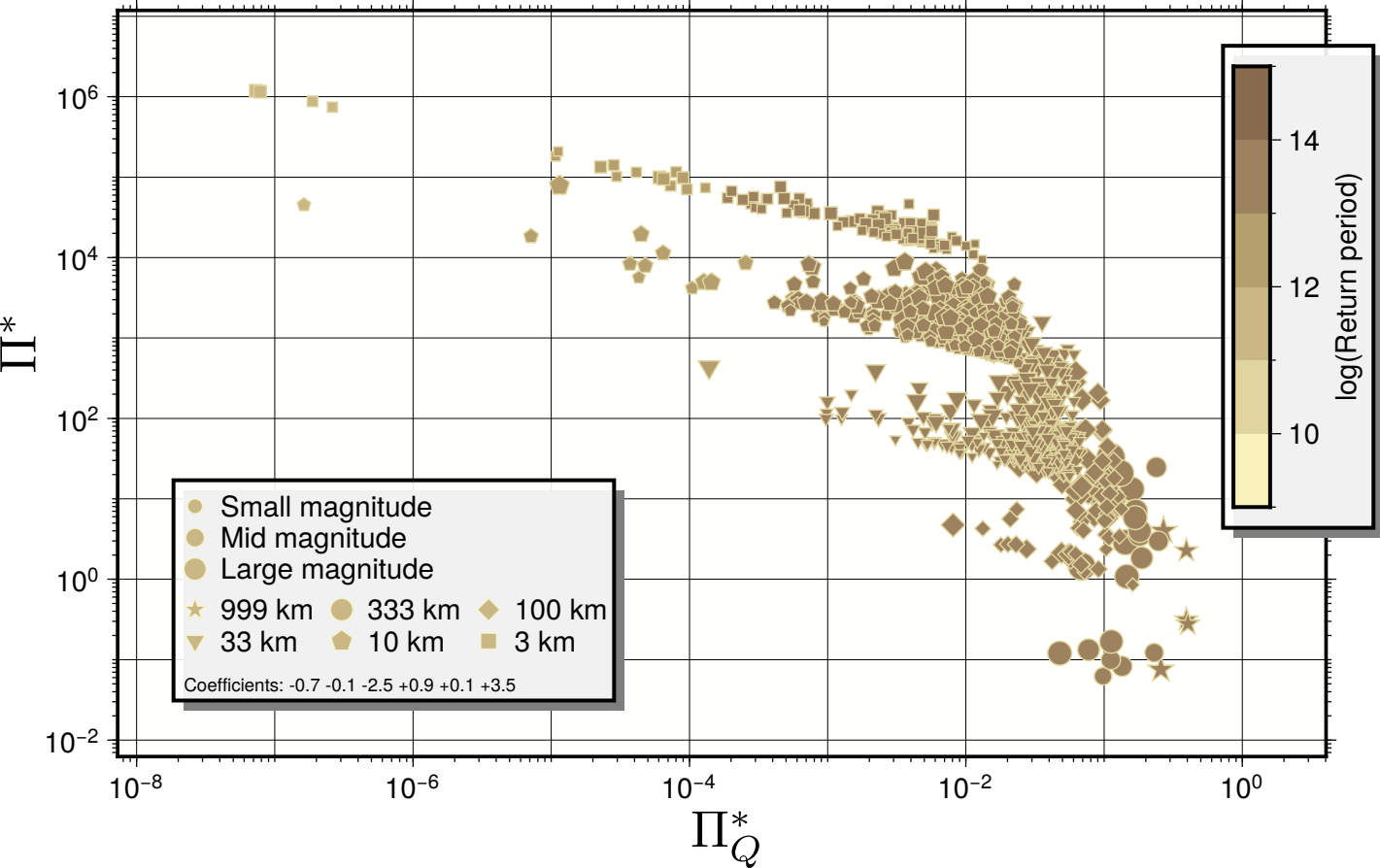


Figure6.

